Mechanical properties of CNTs with S-W defects

A thesis

Submitted to

Department of Mechanical Engineering

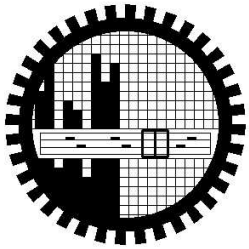

Bangladesh University of Engineering and Technology

by

Md. Zahabul Islam

Under the supervision of

Dr. Monon Mahboob

In partial fulfillment of the

Requirement for the Degree

of

Master of Science in Mechanical Engineering.

July, 2013

DECLARATION

This to certify that the presented paper is the outcome of the accomplishment of the project and thesis on **"Mechanical properties of CNTs with S-W defects"** carried out by Md. Zahabul Islam, student of Mechanical Engineering Department, BUET, Dhaka under the supervision of Dr. Monon Mahboob, Assistant Professor, Mechanical Engineering Department, BUET, Dhaka and it has not been submitted anywhere for any award of degree or diploma.

Name	**Student Number**	**Signature**
Md. Zahabul Islam	0411102088	

SUPERVISOR

Dr. Monon Mahboob
Assistant Professor
Dept. of Mechanical Engineering
BUET, Dhaka-1000.

CERTIFICATE OF APPROVAL

This thesis titled Mechanical properties of CNTs with S-W defects by Md. Zahabul Islam, Roll No: 0411102088P, Session: …….. has been accepted as satisfactory in partial fullfillment of the requirement for the degree of Master of Science in Mechanical Engineering on…….

BOARD OF EXAMINERS

_____ Chairman

Dr. Monon Mahboob
Assistant Professor
Department of Mechanical Engineering
BUET, Dhaka-1000
(Supervisor)

_____ Member

Dr. Md. Ehsan (Ex-Officio)
Professor & Head
Department of Mechanical Engineering
BUET, Dhaka-1000

_____ Member

Dr. Md. Afsar Ali
Professor
Department of Mechanical Engineering
BUET, Dhaka-1000

_____ Member

Dr. Md. Shahnewaj (External)
Assistant Professor
Department of Mechanical and Production Engineering
AUST, Dhaka-1000

ACKNOWLEDGEMENT

I thank my supervisor, Dr. Monon Mahboob, for the great research opportunities and outline he has provided for me, including his extensive suggestions and discussions, and for the encouragement he has always maintained.

I also want to thank Robert L. Lowe and Professor Stephen E. Bechtel at The Ohio state University for their constructive suggestion throughout the work.

LIST OF TABLES

LIST OF FIGURES

ABSTRACT

Although single-walled carbon nanotubes (SWCNTs) are found to have remarkable mechanical properties, a substantial variation in performance data is reported in the literature. These discrepancies may be attributed to the presence of nanoscale defects, among other factors.

In this thesis, the effects of Stone-Wales (SW) defects on the mechanical properties of composites reinforced with SWCNTs are studied using molecular dynamics (MD) simulations. In particular, the effects of Stone-Wales defects on the mechanical properties of SWCNTs and their composites (polyethylene reinforced with SWCNTs) are studied. MD results obtained in the current thesis were corroborated against analytical and atomistic finite element (AFE) results. Our simulations showed that the longitudinal Young's modulus of individual single-walled carbon nanotubes is dependent on the tube structure, the diameter of the nanotube, and the number of Stone-Wales defects. In the present study MD result is compared with FE result. The FE results show good agreement with MD predictions for defect-free SWCNTs, although the accuracy of the AFE results declines for defective nanotubes with diameters less than 9.5 Angstroms.

MOTIVATION

The discovery of carbon nanotubes creates a new dimension in the field of nanotechnology. Being a promising material, different types of advanced materials have been developed from carbon nanotubes. In 1985, Kroto et al. [1] discovered a geometrical form of carbon, C_{60}, called Bucky Fullerene, which is spherical in shape consists of carbon atoms with only hexagonal and pentagonal faces. In 1991, Iijima and Icihashi [2] observed multiple graphene sheets rolled into a tube form, and discovered multi-walled nanobube (MWCNT). Later in 1993, Bethune and his co-workers [3] discovered single-walled nanotube (SWCNT).

Carbon nanotubes (CNTs) possess excellent mechanical properties, such as high Young's modulus and tensile strength. Due to their high aspect ratios, CNTs have much larger surface area than that of the traditional reinforcement fibers. This makes the CNT composites have a much larger interface area than that of the traditional fiber-reinforced composites with the same reinforcement volume fraction. Subsequent investigations have shown that carbon nanotubes (CNTs) has excellent properties, such as exceptionally high elastic properties, large elastic strain, and fracture strain sustaining capability, which seem impossible in the conventional materials [4-10]. CNTs are the strongest fibers among all materials. The Young's modulus of a SWCNT is around 1TPa, which is 5 times greater than steel while the density is only 1.2~1.9 g/cm^3.

Therefore, SWCNTs are regarded as the most promising reinforcement material for the next generation of high-performance structural and multifunctional polymer-based composites.

There is growing evidence that the presence of a small number of defects in a carbon nanotube's (CNT's) atomic structure can result in the degradation of its mechanical properties [5,11]. These defects can appear during CNT growth and purification, composite processing (i.e. chemical functionalization), and under mechanical strains. Although several experimental studies [12,13] have shown the presence of SW defects in CNTs, composites reinforced with SW defective CNTs have not yet been studied. In the current research, the effect of Stone-Wales defects on the mechanical properties of SWCNTs and nanocomposites reinforced with SW defective SWCNTs has been studied using molecular dynamics (MD) simulations as MD simulations provide an affordable alternative to experiments with nano-scale materials.

RESEARCH OBJECTIVES

This research evalutes the mechanical properties of individual carbon nanotubes and carbon nanotube based composites with Stone-Wales defects in CNTs using molecular dynamics (MD) simulation. The primary goals of the current research are:

- Quantifying the degradation of the tensile modulus in defective CNTs,
- Benchmarking FE simulation results for defective CNTs against companion MD simulations,
- Determining the range of applicability of the FE results
- Investigation of the effect of molecular structure (or chirality) and CNT diameter on the mechanical properties.
- Investigation of the elastic properties of the amorphous Polyethylene
- Investigation of the effect of number of Stone-Wales defects on the mechanical properties of composites containing defective carbon nanotube.
- Investigation of the effect of volume fraction on the mechanical properties of composites containing defective carbon nanotube is studied.

NOMENCLATURE

Symbol	Abbreviations
A_{cell}	Cross-sectional area of simulation cell
a	Acceleration of individual atom
$\overrightarrow{a_1}$	Unit vector
$\overrightarrow{a_2}$	Unit vector
$\overrightarrow{C_h}$	Chiral vector
D	Diameter of the carbon nanotube
D_o	Depth of Lennard-Jones potential
d	Carbon bond diameter
E	Young's modulus of C-C bond
E_m	Young's modulus of matrix
$E_{1,CNT}$	Longitudinal Young's Modulus of CNT
F	Axial force
f_{CNT}	Volume fraction of CNT
f_m	Volume fraction of matrix
f_i	Force on individual atom
G	Shear modulus of C-C bond
h_{vdW}	Van-der-Waals separation distance
J	Polar moment of inertia of C-C bond
K	Compressibility
k_R	Bond stretching stiffness
k_θ	Bond in-plane bending stiffness
$k_\emptyset$	Bond torsion stiffness
k_ω	Bond inversion stiffness
k_τ	Bond torsion stiffness for FE analysis
L	Bond length
ΔL	Elongation in bond length

m	Chiral index in Armchair direction
N	Number of particle
n	Chiral index in Zigzag direction
P	Pressure
P_o	Atmospheric Pressure
q_i	Partial charges of a pair of atoms
q_j	Partial charges of a pair of atoms
R	Radius of the CNT
r_i	Position of individual atom
$\dot{r}_i$	Velocity of individual atom
$\ddot{r}_i$	Acceleration of individual atom
Δr	Bond stretching increment
T	Temperature
t	time
Δt	timestep
t_w	Wall thickness of the CNT
U_{el}	Electrostatic energy
U_F	Bond stretching energy
U_M	Bond bending energy
U_R	Bond stretching energy
U_T	Bond torsion energy
U_{TOT}	Total potential Energy
U_{vdW}	Van-der-Waals energy
U_θ	Bond bending energy
U_ϕ	Bond torsion energy
U_ω	Bond inversion energy
V	Volume
v_i	Velocity of individual atom
Y	Young's modulus of CNT for FE analysis

Greek symbols

α	In-plane rotational angle
β	Angle of twist
ϵ	Strain
ε	Dielectric constant
θ	Deformed in-plane angles between two bonds
θ_o	equilibrium in-plane angles between two bonds
$\Delta\theta$	Bond angle change
λ	Scaling factor
σ	Stress
τ	Relaxation time constant
χ	deformed inversion angles
χ_o	equilibrium inversion angles
$\emptyset$	torsion angle
$\Delta\emptyset$	Bond twisting change

1. INTRODUCTION

1.1 Nanotechnology

Nanoscale science and engineering offer the possibility for revolutionary advances in both fundamental science and technology. At its basic level, nanoscale science is the study of novel phenomena and properties of materials that occur at nano length scales, which is the size of atoms and molecules. Nanotechnology is the application of nanoscience and engineering methods to produce novel materials and devices.

In 1959, a lecture given by Richard Feynman is considered to be the first scientific discussion on nano science and nanotechnology [14]. In 1982 invention of scanning tunneling microscopy (STM) [15] and in 1986, atomic force microscopy (AFM) [16] invented by a group of researchers in IBM lead by Gerd Binnig, has accelerated the research at nanoscale. Binnig and Heinrich Rohrer were awarded the Nobel Prize in Physics in 1986 for the invention of STM. These inventions gave the researchers ability to observe individual atoms and manipulate them, which lead Harold Kroto, Robert Curl, Richard Smalley, and Sean O'Brien to discover the buckyball, and they were awarded the 1996 Nobel Prize in Chemistry for their discovery [17]. A giant leap in nanotechnology is the discovery of carbon nanotube by Sumio Iijima in 1991 [2]. Due to this revolutionary discovery, Iijima was awarded the Kavli Prize in nanoscience in 2008.

1.2 Carbon nanotube

Carbon nanotubes (CNTs) are allotropes of carbon with a cylindrical nanostructure. These cylindrical carbon molecules have exceptional properties, which are valuable for nanotechnology, electronics, optics and other fields of materials science and technology. In particular, owing to their extraordinary thermal conductivity and mechanical and electrical properties, carbon nanotubes find applications to various structural materials.

A Carbon nanotube (CNT) is basically a cylinder with a single layer of atoms where each carbon atom is bonded to three other carbon atoms via covalent bonds in a hexagonal lattice structure. Therefore, CNT can be viewed as a graphene sheet rolled up to the shape of a cylinder. Based on the orientation of the C-C bond CNT can be classified as:

i) Chiral CNT

ii) Achiral CNT

Orientation of the C-C bond is characterized by,

Chiral vector, $\overrightarrow{C_h} = n\overrightarrow{a_1} + m\overrightarrow{a_2}$, 1.2(a)

Diameter, $d = \frac{2.46}{\pi}\sqrt{(m^2 + n^2 + mn)}$ (in Angstrom) 1.2(b)

Chiral angle, $\theta = sin^{-1}(\frac{\sqrt{3}}{2}\frac{m}{\sqrt{m^2+n^2+mn}})$ 1.2(c)

where $\overrightarrow{a_1}$ and $\overrightarrow{a_2}$are unit vectors in the two dimentional hexagonal graphene sheet, m and n are chiral indices. Angle between chiral vector $\overrightarrow{C_h}$ and unit vector $\overrightarrow{a_1}$ is called chiral angle (Fig. 1.1). Nanotubes having chiral angle of 0^o and 30^o are called zigzag and armchair, respectively, while nanotubes having chiral angles between 0^o and 30^o are called chiral CNTs. SWNTs are uniquely defined by the integer pair (*n,m*).

In case of Zigzag nanotube, m=0, Armchair nanotube n=m and for chiral nanotube $n \neq m$. Thus Zigzag and armchair CNTs are represented by the integer pairs (*n, 0*) and (*n, n*) respectively, while chiral CNTs are represented by (*n,m*). For zigzag CNTs *m* takes the value of zero, otherwise chiral indices *n* and *m* take values greater than or equal to 3.

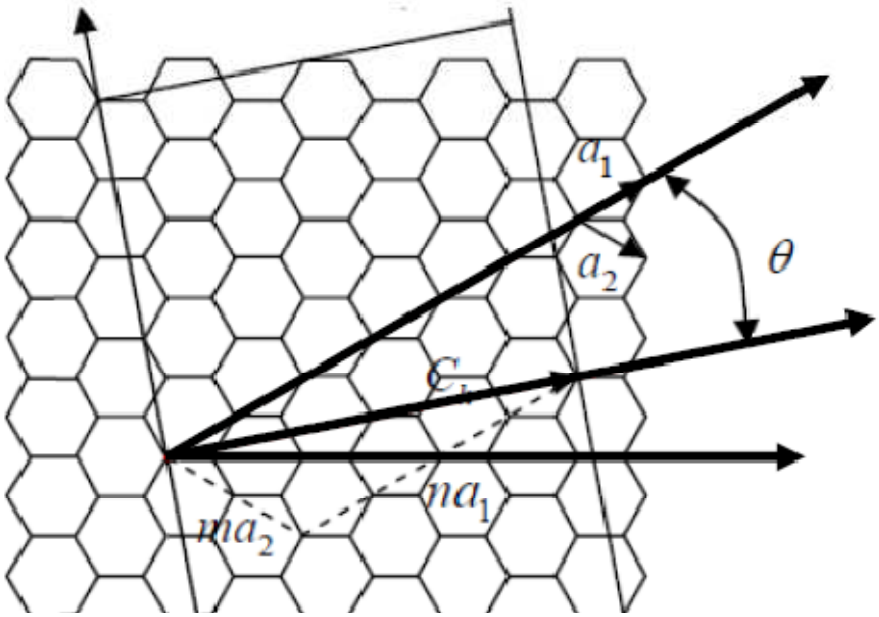

Fig. 1.1: Chirality of CNT

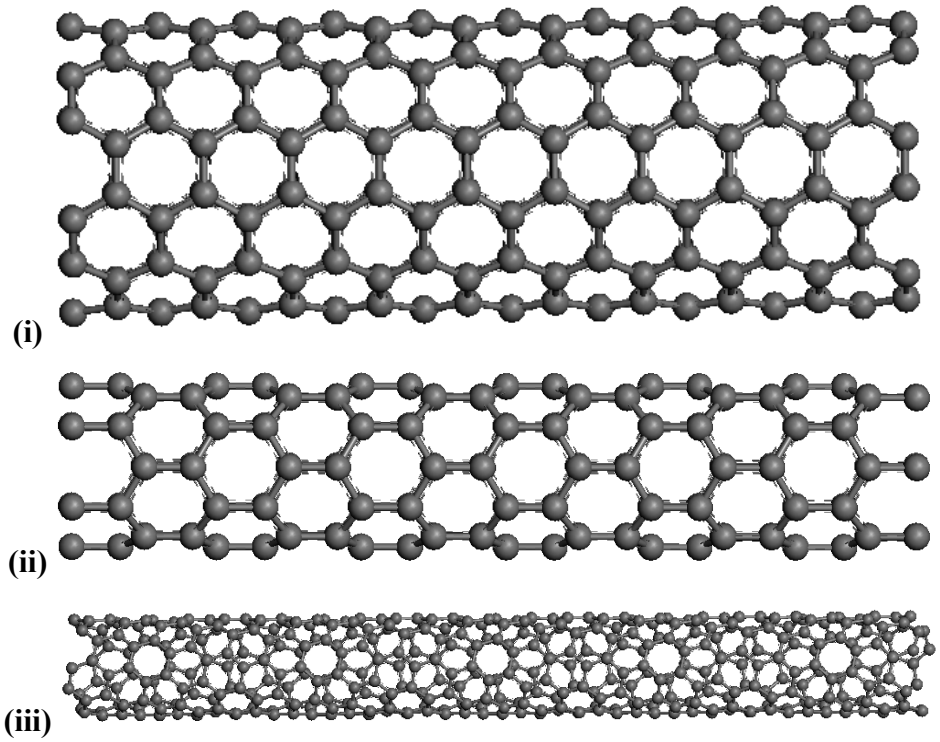

Fig. 1.2: Different types of CNTs based on chirality (i) Armchair (6,6) (ii) Zigzag (6,0) (iii) Chiral (6,3).

Depending on the number of wall in the CNT, the following categories of CNT can be found:

i) Single wall carbon nanotube (SWCNT)

ii) Multi wall carbon nanotube (MWCNT)

SWCNT consists of a single layer of graphene layer rolled into a tube (Fig. 1.2). In case of MWCNT more than one layer of graphene rolled into a tube and each tube wall are separated by Van-der-Waals distance (Fig. 1.3). MWCNT contains several CNTs inserted within one another with an inter-wall spacing of approximately 0.34 nm[18]. Walls of MWNTs are bonded by the weak van der Waals forces which are defined as attractive or repulsive forces between atoms or molecules.

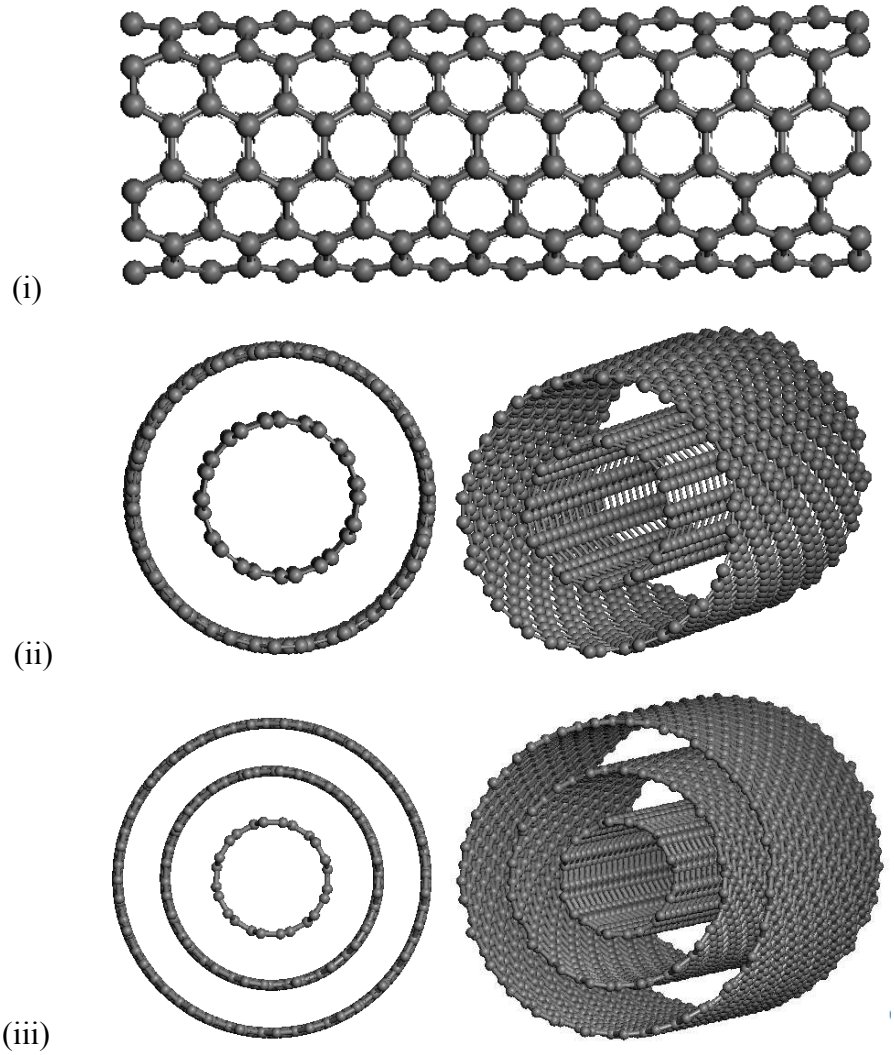

Fig. 1.3: CNTs based on number of walls (i) SWCNT (ii) DWCNT (iii) TWCNT

There is growing evidence that the presence of a small number of defects in a carbon nanotube's atomic structure can result in the degradation of its mechanical properties [5,11]. Based on defects those arise during the CNT growth purification and composite processing, CNT can be classified as:

i) Pristine CNT

ii) Defective CNT

According to the evidence that has mentioned above, CNTs can be categoried as pristine and defective CNTs. These defects can appear during CNT growth and purification composite processing (i.e. chemical functionalization) and under mechanical strains. Types of defects can

be classified as vacancy (i.e atom missing) and Stone-Wales (i.e pentagon-heptagon pair) defects.

Vacancy defects, i.e., defects resulting from missing carbon atoms can cause significant changes in electronic, mechanical, and magnetic properties of CNT. These defects have already received considerable attention, in part because they can be readily induced by either electron or ion irradiation. One of the most intensively studied defects is the 5-7-7-5 dislocation formed by a Stone-Wales (SW) transformation. Stone-Wales defects are composed of two pentagon–heptagon pairs, and can be formed by rotating a sp^2 bond by 90˚ (Fig. 1.4). Experimental observations have revealed that topological defects such as the 5-7-7-5 Stone-Wales defect are stable, commonly present in nanotubes [19,20], and play an important role in the mechanical properties of SWCNTs. A SW defect, which is made by a 90º rotation of a single carbon-carbon bond, emerges during the growth process of CNTs and other curved graphitic structures, like graphene [21]. This kind of defect can be introduced to the system, i.e, by single electron irradiation [22], or by exerting stress and tension to CNTs [23].

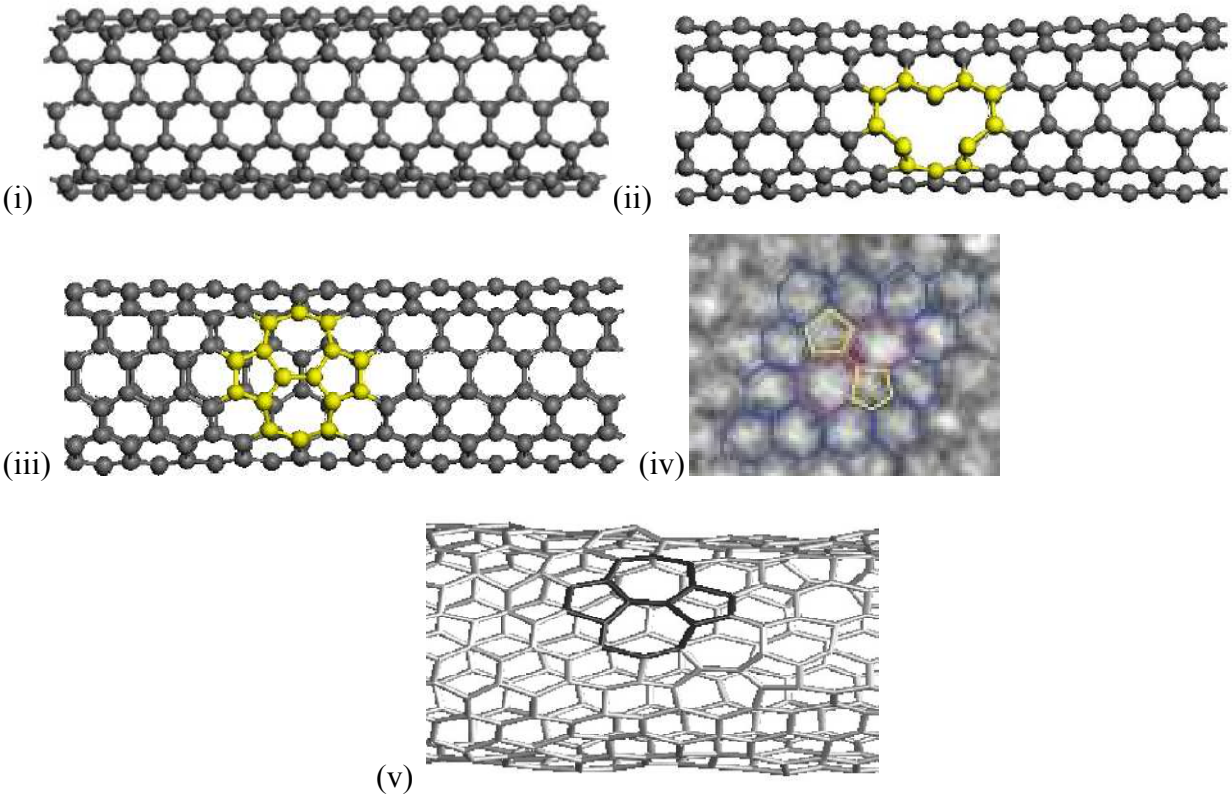

Fig. 1.4: (i) Pristine CNT (ii) SWCNT with Vacancy defects (iii) SWCNT with Stone-Wales defects (iv) Experimentally observed SW defects (ref. [22]) (v) SW defects (ref. [23]).

2. LITERATURE REVIEW

Single-walled carbon nanotubes (SWCNTs) are attractive materials for emerging applications in advanced electronics, biotechnology, and environmental technology, to name a few. The exceptional mechanical properties exhibited by SWCNTs have stimulated great interest and extensive research since their discovery by Iijima S. et. al. [2] in 1991. Experiments [4,6,11] report longitudinal Young's moduli of single-walled carbon nanotubes as high as 1.8 TPa. Other researchers have applied computational methods such as molecular dynamics (MD) simulations [24-26] and *ab initio* methods [27-29] to determine the tensile modulus of SWCNTs. In these experimental and computational studies, the reported values of the tensile modulus vary substantially from study to study.

Nano reinforcement of engineering materials can impart excellent structural and physical properties benefits without adding significant weight [30,31]. The elastic properties of SWCNTs and that of polymer composites containing SWCNTs have been studied through theoretical, experimental and computational method [32-34]. The ultra-high stiffness and low specific weight make single-walled carbon nanotube (SWCNT) a viable reinforcement in high performance composites [35] for emerging applications in advanced electronics, biotechnology, and environmental technology, to name a few. Enhancements in elastic modulus and strength have been achieved by adding small amounts of CNTs to polymer matrix in experiments [36-38]. Frankland et.al. [39,40] have studied the stress-strain behavior of nanotubes in polyethylene and the influence of chemical cross-linking between the nanotube and the polyethylene matrix. Due to the presence of matrix-fiber cross-links the load transfer between the nanotube and the matrix was shown to improve considerably. Lei [41] et. al tested the mechanical properties of CNT/epoxy resin composites at normal and elevated temperatures. Dalton [42] et. al studied the effect of volume fraction of SWCNT on mechanical properties of SWCNT/Si composites.

There is growing evidence that the presence of a small number of defects in a carbon nanotube's (CNT's) atomic structure can result in the degradation of its mechanical properties [2,5]. These defects can appear during CNT growth and purification [43,44], composite processing (i.e. chemical functionalization) [45,12], and under mechanical strains [13].

One of the most intensively studied defects is the 5-7-7-5 dislocation formed by a Stone-Wales (SW) transformation. Stone-Wales defects are composed of two pentagon–heptagon pairs, and can be formed by rotating a sp^2 bond by 90°. Experimental observations have revealed that topological defects such as the 5-7-7-5 Stone-Wales defect are stable, commonly present in nanotubes [46,47], and play an important role in the mechanical properties of SWCNTs [12,13].

Previously, carbon nanotubes have been modeled as a continuum [48-51], where the homogeneous mechanical properties of the CNT have been derived from a cylindrically shaped representative volume element. However, these continuum models are not suitable for modeling nanotubes with defects, as they assume the material to be perfect. A recent approach for modeling defective CNTs is atomistic modeling [51], where the chemical bonds between carbon atoms are modeled using elastic beam elements. Atomistic finite element (FE) analysis is less computationally expensive than molecular dynamics, but the approach is phenomenological and dependent on accurate data obtained from MD simulations.

Tserpes et al. [51,52] simulated carbon–carbon chemical bond based on molecular mechanics approach. In their work, they used an elastic beam element to represent the chemical bonds. Fan et al. built an FE model for both SWCNTs and MWCNTs [53]. His approach was based on elastic carbon-bond beam-like representation and a linkage between the beam sectional stiffness parameters and constants of the force field. Wan and Delale [54] studied the buckling of SWCNTs with emphasis on the out-of-plane deformation of the bonds by considering a rectangular cross-section for the beam elements.

Scarpa et. al [55] have shown that Mechanical properties of non-reconstructed vacancy defective SWCNTs are qualitatively and quantitatively different from the pristine configurations. The defective nanotubes show a slight reduction in axial stiffness but large variations of Poisson's ratio outside the elastic bounds for isotropic materials, depending on the locations of the vacancies.

Lu et. al [13] have studied the effects of randomly distributed SW defects on the mechanical properties of SWCNTs using atomistic simulation (AS) and showed that the stiffness, ultimate strength and ultimate strain of the SWCNTs decrease as the average number of defects increases.

Xiao et. al [56] studied the effects of interactions of multiple SW defects on mechanical properties of graphene sheets and carbon nanotubes using atomistic FE methods.

3. THEORY

3.1 MOLECULAR DYNAMICS SIMULATION

Molecular dynamics (MD) simulation is a computer simulation technique employed widely in analyzing atomistic systems. Computer simulation is a powerful and modern tool for solving scientific problems as numerical studies can be performed for new materials without synthesizing them. One of the aims of computer simulation is to reproduce experiment to elucidate the invisible microscopic details and further explain experiments. On the other hand, simulation can also be used as a useful predictive tool. The most widely used simulation method for molecular systems is molecular dynamics. Molecular dynamics is the most detailed molecular simulation method [57] which computes the motions of individual molecules. Coupled Newton's equations of motion, which describe the positions and momenta, are solved for a large number of particles of the bulk system.

Molecular Dynamics simulations are in many respects very similar to real experiments. We perform a real experiment by preparing a sample of the material that we wish to study then connect this sample to a measuring instrument (e.g., a thermometer, manometer etc.), and we measure the property of interest during a certain time interval. When measurements are subject to noise (as most measurements are), we average for the longer time to obtain the more accurate measurements. Molecular Dynamics simulation follows the same methodology. We prepare a sample by selecting a model system consisting of particles and we solve Newton's equations of motion for this system until the properties of the system no longer change with time (i.e equilibriation). After equilibration, we perform the actual measurement (i.e mechanical, electrical, optical or other properties).

3.1.1 Molecular Dynamics Simulation Algorithm

Molecular dynamics uses Newton's equations of motion to calculate the trajectory (the coordinates and velocities for a complete dynamics run are called the trajectory) of atoms in any system. The primary equations of molecular dynamics simulation can be obtained from Newtonian Mechanics:

$$\dot{r}_i(t) = \frac{dr_i}{dt} = v_i \qquad (3.1)$$

$$m_i \ddot{r}_i(t) = m_i \frac{d^2 r_i}{dt^2} = -\frac{dU(r_1, r_2, r_3 \ldots\ldots\ldots\ldots r_N)}{dr_i} = f_i(t) \quad (3.2)$$

Let us assume that the above system of equations is obtained at time t, then Finite difference method is used to update the current trajectory after solving the equations of motion. Here U is the potential energy of the system defined by forcefields.

3.1.1.1 Forcefields

Forcefield is a mathematical description of the potential energy of a system of interacting atoms. Parameters in forcefield are derived from both experimental work and high-level quantum mechanical calculations, so they are empirical in nature. Researchers have derived various forcefields to simulate various molecular systems.

From the molecular mechanics viewpoint, a carbon nanotube can be regarded as a large molecule consisting of carbon atoms in a hexagonal ring array. The resultant force on each carbon nucleus is the sum of the forces generated by the electrons and electrostatic forces between the nuclei themselves. These atomic forces, which are an integral part of MD models, are conservative and hence can be obtained from a total potential energy function (or force field) that depends on the relative positions of the nuclei.

In this paper, following the seminal work of Rappe et al. [58], the total potential energy U_{TOT} of the bond between two atoms consists of contributions from bond stretchingU_R, in-plane bond angle bending U_θ, torsion U_ϕ, inversions U_ω, van der Waals interactions U_{vdW}, and electrostatic interaction U_{el}, i.e.,

$$U_{TOT} = U_R + U_\Theta + U_\phi + U_\omega + U_{vdW} + U_{el} \quad (3.3)$$

with the first four terms of Eq. (3.3) representing bonded interactions and the last two terms representing non-bonded interactions. Again following [58], we model the energy due to bond stretching with a quadratic polynomial (similar to a harmonic oscillator) as:

$$U_R = k_R(r - r_o)^2 \quad (3.4)$$

in-plane bond angle bending with a three-term Fourier cosine expansion as

$$U_\theta = k_\theta(C_o + C_1 \cos\theta + C_2 \cos 2\theta) \quad (3.5)$$

where

$$C_2 = 1/(4\sin^2\theta_o), C_1 = -4C_2\cos\theta_o, C_o = C_2(2\cos^2\theta_o + 1) \quad (3.6)$$

bond torsion and inversion (out-of-plane bending) with one-term Fourier cosine expansions

$$U_\emptyset = k_\emptyset(1 \pm \cos n\emptyset) \quad (3.7)$$

$$U_\omega = k_\omega[1 + \cos(n\chi - \chi_o)] \quad (3.8)$$

Van-der-Waals interactions with a Lennard-Jones potential

$$U_{vdW} = D_o[\left(\frac{r_o}{r}\right)^{12} - 2\left(\frac{r_o}{r}\right)^{6}] \quad (3.9)$$

and electrostatic interactions with a Coulomb-type potential

$$U_{el} = \frac{q_i q_j}{\varepsilon r_o} \quad (3.10)$$

In Eqs. (3.3)-(3.10), r and r_o are the deformed and equilibrium bond lengths, respectively; θ and θ_o are the deformed and equilibrium in-plane angles between two bonds; $\emptyset$ is the torsion angle; χ and χ_o are the deformed and equilibrium inversion angles; k_R, k_θ, $k_\emptyset$, and k_ω are the rigidities corresponding to stretching, in-plane bending, torsion, and inversion; D is the depth of the Lennard-Jones potential; ε is the dielectric constant; q_i and q_j are the partial charges of a pair of atoms; and n is an integer. The numerical values of these parameters are atom-dependent, for which detailed values can be found in [58].

3.1.1.2 Numerical solution of equations of motion

The standard method of solving an ordinary differential equation such as Eqn 3.1 and 3.2 numerically is the finite-difference method. The general idea is as follows. Given the initial coordinates and velocities and other dynamic information at time t, the positions and velocities at time t+Δt are calculated. The time step Δt depends on the integration method as well as the system itself. Molecular dynamics is usually applied to a large model. To generate the correct

statistical ensembles, energy conservation is also important. Thus, the basic criteria for a good integrator for molecular dynamics simulations are:

(a) It should be fast
(b) It should require little CPU memory.
(c) It should allow relatively long timestep.
(d) easy to implement

There are many techniques to integrate the equation of motion. Among them velocity verlet integrator is widely used in MD simulation.

3.1.1.2.1 Velocity Verlet algorithm

Initial position, r(t) and velocity, v(t) are known. Acceleration, a(t) can be determined from the potential energy function (i.e forcefield) at time t. Position, r(t+Δt) at time t+Δt, can be determined from the Taylor's series expansion as follows:

$$r(t + \Delta t) = r(t) + v(t).\Delta t + \frac{1}{2}a(t).(\Delta t)^2 + H.O.T \quad (3.11)$$

$$a(t + \Delta t) = \frac{f(t+\Delta t)}{m} \quad (3.12)$$

$$v(t + \Delta t) = v(t) + \frac{1}{2}[a(t) + a(t + \Delta t)].\Delta t + H.O.T \quad (3.13)$$

3.1.1.3 Ensembles

An ensemble is a collection of all the possible states of a real system. Several methods are available for controlling temperature and pressure. Depending on which state variables (the energy E, enthalpy H (that is, U+PV), number of particles N, pressure P, stress S, temperature T, and volume V) are kept fixed, different statistical ensembles can be generated as follows:

Constant Number of particles, constant temperature and constant pressure (NPT)
Constant Number of particles, constant temperature and constant volume (NVT)
Constant Number of particles, constant volume and constant energy (NVE)
Constant Number of particles, constant pressure and constant enthalpy (NPH)

NPT ensemble

The constant number of particles, constant-temperature, constant-pressure ensemble (NPT) allows control over both the temperature and pressure. The unit cell vectors are allowed to change, and the pressure is adjusted by adjusting the volume. Pressure can be controlled by the Berendsen, Andersen, or Parrinello-Rahman method. Temperature can be controlled by any method available i.e Nose-Hoover, Andersen, or Berendsen. NPT is the ensemble of choice when the correct pressure, volume, and densities are important in the simulation.

NVT ensemble

NVT ensemble is obtained by controlling the temperature through direct temperature scaling during the initialization stage and by temperature-bath coupling during the data collection phase. Temperature controlled MD simulation is important in several types of systems.

NVE ensemble

NVE the pressure and temperature is not controlled during the simulation. The main objective is to conserve the energy. However, this might cause the pressure or temperature overshoot during time integration process. Typically, a system with higher stability is suitable for NVE. Thermodynamically systems following NVE ensemble are insulated from the surrounding environment

NPH ensemble

Enthalpy H, which is the sum of U and PV, is constant when the pressure is kept fixed without any temperature control. Although the temperature is not controlled during NPH dynamics, it is possible to use these conditions during the equilibration phase of simulation. For this purpose, it is possible to hold the temperature within specified tolerances by periodic scaling of the velocities.

3.1.1.4 Methods of Pressure Control

The pressure can be changed by changing the coordinates of the particles and the size of the unit cell. The Berendsen method couples the system to a pressure bath to maintain the pressure at a certain target (Fig. 3.1). The strength of coupling is determined by both the compressibility of the

system (using a user-defined variable K) and a relaxation time constant (a user-defined variable τ). At each step, the x, y, and z coordinates of each atom are scaled by the factor:

$$\lambda = \sqrt[3]{(1 + \frac{\Delta t}{\tau} K[P - P_o])} \tag{3.14}$$

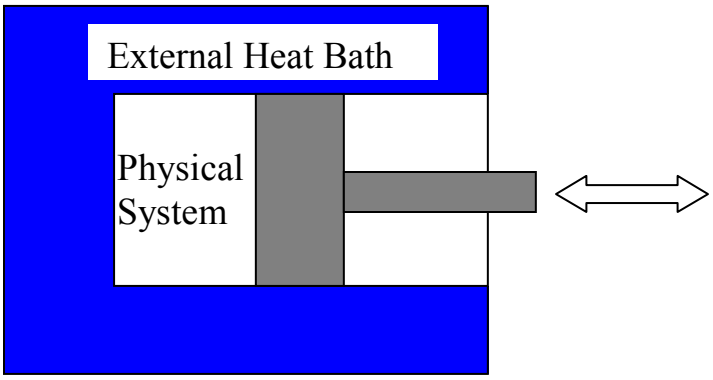

Fig. 3.1 Physical system coupled to external heat bath under NPT ensemble

The first step in molecular dynamics simulation involves attainment of equilibrium state of materials. In order to attain such equilibrium state it requires to achieve energy stabilized state at a predefined temperature, and minimum initial stress state of the periodic structure at that temperature. In the present study NVT, NPT and NVE ensembles were used to carry out the simulations in order to accomplish such equilibrium state. Depending on the molecular models different ensembles were used in the present study. For CNTs simulation all the simulations were conducted under NPT ensemble. Whereas for polymer matrix and nanocomposite simulation, all these three ensembles (NVT, NPT and NVE) were used to achieve energy stabilized and minimum initial stress state of the systems.

3.2 ATOMISTIC FINITE ELEMENT SIMULATION:

In this section, we employ a molecular-continuum analogy to develop a 3-D atomistic finite element (FE) model using ANSYS® commercial FE software. To create the atomistic FE model, nodes are placed at the locations of carbon atoms in the CNT, and the covalent bonds between them are modeled using three-dimensional elastic beam elements with uniform circular cross-sectional areas (Fig. 3.2).

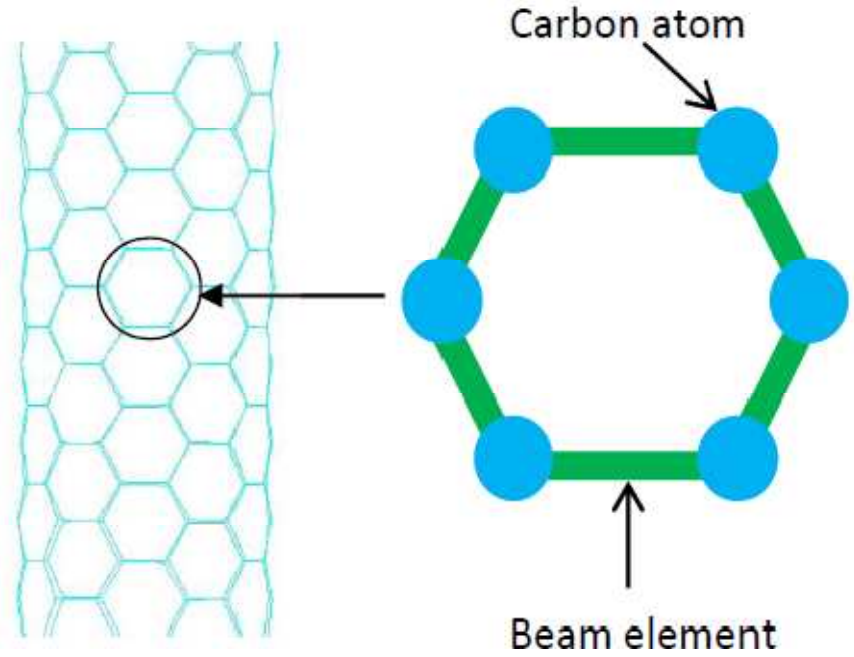

Figure 3.2: Schematic diagram of the finite element model of a CNT.

The resulting FE model is solved in two key steps: In the first step, the concept of energy equivalence is used to obtain the elastic properties (Young's modulus and shear modulus) and geometry (diameter and length) of the elastic beam elements. This data, in turn, serves as input to the FE code, which is used to determine the force-deformation behavior of the atomistic CNT model in an uniaxial tension test.

3.2.1 Elastic properties and dimensions of the beam elements

In what follows, we illustrate our derivation of the material properties and dimensions of the elastic beam elements. This procedure involves two sub-steps: First, using the concept of energy equivalence between a carbon-carbon bond and an elastic beam, we obtain the axial, flexural,

and torsional rigidities of the bonds in terms of the continuum-level material and geometric properties of the beams. Next, using reported values of these bond rigidities in the molecular dynamics literature, we deduce the elastic constants and geometry of the beam elements.

Following Odegard et. al. [48] and Li and Chou [49], we proceed by recalling the energies in a carbon-carbon bond, which can be obtained from Eqs. (3.3) as

$$U_{TOT} = U_R + U_\theta + U_\tau \tag{3.15}$$

$$U_R = \frac{1}{2} k_R (\Delta r)^2 \tag{3.16}$$

$$U_\theta = \frac{1}{2} k_\theta (\Delta \theta)^2 \tag{3.17}$$

$$U_\tau = U_\phi + U_\omega = \frac{1}{2} k_\tau (\Delta \emptyset)^2 \tag{3.18}$$

where the energies due to torsion and inversion have been merged and non-bonded interactions have been neglected. In (3.16)-(3.18),Δr, $\Delta\theta$, and $\Delta\emptyset$ represent the bond stretching increment, the bond angle change, and the bond twisting change, respectively; and k_R, k_θ, and k_τ represent the rigidities associated with stretching, flexure, and torsion of the chemical bonds, respectively. According to structural mechanics, the total strain energy of a beam consists of contributions from stretching, flexure, and torsion. A new formulation using Timoshenko beam for the equivalent mechanical properties (Young's modulus, shear modulus and Poisson's ratio) of the C–C bond of CNTs under tensile and bending small deformations have been reported in [52]. Assuming C-C bond as pure 3-D beam element strain energy associated with tension, torsion and bending can be expressed as follows [41,48]:

The strain energy U_F due to stretching induced by an axial load is

$$U_F = \frac{1}{2} \frac{EA}{L} (\Delta L)^2 \tag{3.19}$$

where A is the cross-sectional area, L is the length, $\Delta L$is the elongation, and E is the Young's modulus of the beam. The strain energy U_M due to flexure induced by a bending moment is

$$U_M = \frac{1}{2}\frac{EI}{L}(2\alpha)^2 \tag{3.20}$$

where I is the area moment of inertia and α is the in-plane rotational angle of the beam ends. The strain energy U_T due to torsion induced by a torque is

$$U_T = \frac{1}{2}\frac{GJ}{L}(2\beta)^2 \tag{3.21}$$

where J is the polar moment of inertia, β is the angle of twist, and G is the shear modulus of the beam.

Invoking the concept of energy equivalence between the carbon-carbon bond and the elastic beam (Fig. 3.3), the axial, flexural, and torsional rigidities of the bond can be written in terms of the continuum-level material properties and geometric parameters of the beam, i.e.,

$$k_R = \frac{EA}{L} \tag{3.22}$$

$$k_\theta = \frac{EI}{L} \tag{3.23}$$

$$k_\tau = \frac{GJ}{L} \tag{3.24}$$

Using Eqs. (3.22)-(3.24) and noting the uniform circular cross-sectional area of the elastic beam element, its diameter d, Young's modulus E, and shear modulus G, are found to be

$$d = 4\sqrt{\frac{k_\theta}{k_R}} \tag{3.25}$$

$$E = \frac{k_R^2 L}{4\pi k_\theta} \tag{3.26}$$

$$G = \frac{k_R^2 k_\tau L}{8\pi k_\theta^2} \tag{3.27}$$

For the particular values of the bond rigidities, we employ $\mathrm{k_\theta} = 8.79 \times 10^{-10}\mathrm{N.nm/rad^2}$, obtained from MD simulations of CNTs as reported in [50].The carbon-carbon bond length L is

1.42 Å; we take this to be the length of the beam. Then, $k_\theta = 8.79 \times 10^{-10}\text{N.nm/rad}^2$, $E = \frac{k_R^2 L}{4\pi k_\theta}$ using d=1.479 Å obtained from Eq. (3.25), the cross-sectional area, Young's modulus, and shear modulus of the beam are found to be 1.69×10^{-20} m^2, 5.49 TPa, and 0.871 TPa, respectively.

Before using the BEAM4 element properties, the dimensions of the parameters stated above should be further adjusted to avoid digits overflow/underflow error during the computation performed by ANSYS®. Thus, dimensions were adjusted as follows [59]:

$$L_{in} = 10^{10}L, \quad F_{in} = 10^{20}F \tag{3.28}$$

where the original dimensions of length L and force F are in meter (m) and Newton (N) respectively, and the subscript "in" denotes the real input values. In the present study, for SWCNT (6,6) length, L was chosen as 81.4Å and applied force was 12 nN.

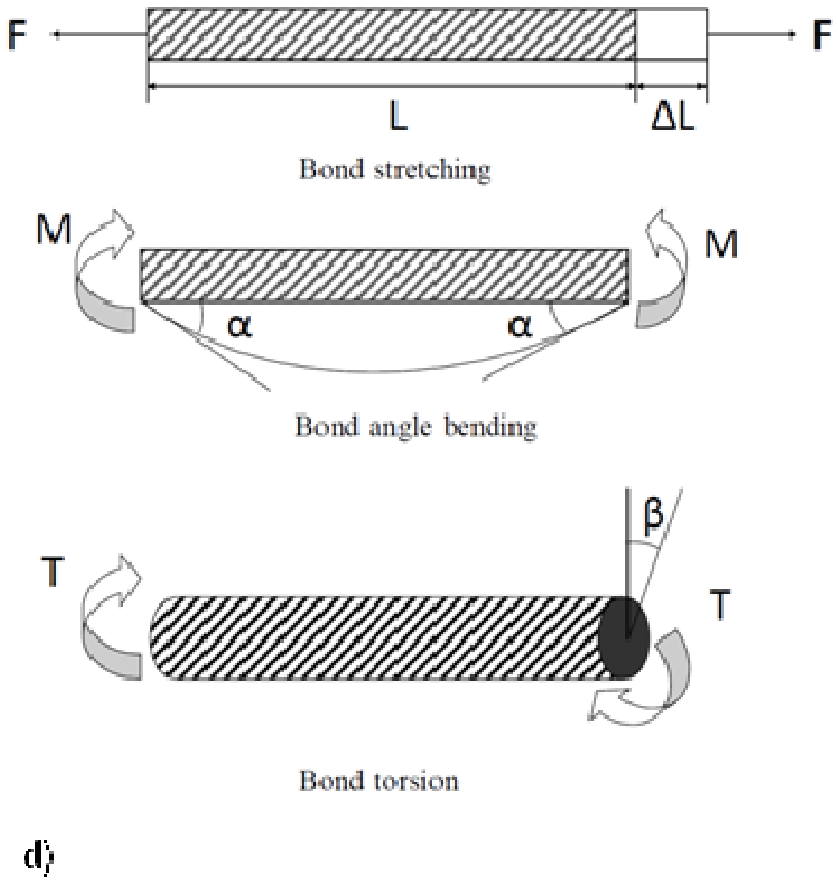

Figure 3.3: Bonded interactions in molecular mechanics: a) bond stretching, b) bond angle bending, and c) bond torsion. Analogous deformations of an elastic beam in structural mechanics: d) extension, flexure, and torsion.

4. MECHANICAL PROPERTIES

4.1 Molecular Dynamics Simulation

In general, the stress in a solid is defined as the change in the internal energy (in the thermodynamic sense) with respect to the strain per unit volume. For example, at the continuum level, the stress, σ and Young's modulus, E for a linear-elastic material is [60]:

$$\sigma = \frac{1}{V}\frac{\partial U}{\partial \in} \tag{4.1}$$

$$E = \frac{1}{V}\frac{\partial^2 U}{\partial \in^2} \tag{4.2}$$

where, V denotes the volume of the solid, U is the total internal energy, ϵ is the applied strain. In order to determine the stress and Young's modulus, small strains were applied to the periodic structure of the CNT and nanocomposite by uniformly expanding the dimensions of the periodic structure in the direction of deformation. Then the new coordinates of the atoms were re-scaled to fit within the new dimensions. Keeping the lattice parameters fixed, the energy of the structure was measured. This method to determine the energy increment in each step was repeated for a series of strains. In the current research 0.005 strains was applied in each step in the longitudinal direction of the nanotubes and composite systems. Following this method strain was applied up to 0.03(i.e 3%). By calculating energy, eqn. (4.1) and eqn. (4.2) was used to determine stress and Young's modulus of CNT and composite systems.

The SWCNT (6,6) with an outside diameter of 8.14 Å is treated as a solid beam [61]. Thus for the SWCNT-PE nanocomposite volume fraction can be determined from the following equation,

$$f_{CNT} = \frac{\pi(R+\frac{h_{vdW}}{2})^2}{A_{cell}} \tag{4.3}$$

where, f_{CNT}, R, h_{vdW} and A_{cell} represent volume fraction of the nano composite, radius of the SWCNT, equilibrium van der Waals separation distance between the SWCNT and the matrix and cross-sectional area of the simulation cell respectively. The rule of mixtures was applied in order to compare the results obtained from MD simulations. Longitudinal Young's modulus of

the nanocomposite under constant-strain conditions can be obtained from rule of mixtures using the following form [62]:

$$E_1 = E_{1CNT} f_{CNT} + E_m f_m \tag{4.4}$$

and

$$f_{CNT} + f_m = 1 \tag{4.5}$$

where $E_1, E_{1CNT}, f_{CNT}, E_m$ and f_m represent longitudinal Young's modulus of the nanocomposite, longitudinal Young's modulus of the SWCNT, volume fraction of the SWCNT, Young's modulus of the matrix and volume fraction of the matrix, respectively.

4.2 Atomistic FE simulation

A 3-D atomistic FE model is developed in ANSYS®. To calculate the longitudinal Young's modulus of the SWCNTs, a uniaxial tension test was simulated. In the simulation, one end of the nanotube was fixed, and the other end was subjected to a uniform longitudinal tensile load. By measuring the resulting longitudinal displacement of the SWCNT, the Young's modulus of the nanotube was determined using Hooke's law (see section 5.3).

5. MODELING AND SIMULATION

5.1 Modeling of carbon nanotubes-polyethylene nanocomposites and their constitutes

5.1.1 Molecular dynamics modeling

Molecular dynamics (MD) modeling provides the motions of individual particles as a function of time [51]. The two basic tenets of standard molecular dynamics simulations are [63-65]:

(1) Molecules or atoms are described as a system of interacting material points, whose kinematics is described by vectors of instantaneous positions and velocities. The atomic kinematics is governed by the evolution of the inter atomic forces, as described in Section 3.1.

(2) The mass of the system is conserved.

The initial positions and velocities of the atoms are the initial conditions required by the MD simulation. The MD simulation in the present work involves NPT dynamics as discussed in Section 3.1. Our objective is to determine the elastic or engineering constants of defective single-walled carbon nanotubes with molecular structure or chirality (4,4), (5,5), (6,6), (7,7), and (8,8).

5.1.1.1 Types of defects

Stone-Wales defects (Fig. 5.1) are the most commonly observed topological defects in SWCNTs [13,14,45]. Stone-Wales defects are also called pentagon-heptagon pair defects (or 5-7-7-5 defects). The present study focused on 0, 1, 2, 3, 4, and 5 Stone-Wales defects in SWCNTs with chiralities (4,4), (5,5), (6,6), (7,7), and (8,8). In the present study we introduced SW defects according to the following sequence in the nanotube: The first SW defect is created on the wall at the center of the nanotube. The second and third SW defects are created at the same axial coordinate on opposite sides of the wall. In case of four and five number of defects, a similar sequence is followed at an axial distance of 0.246 nm from the location of the first SW defect as shown in Fig. 5.2.

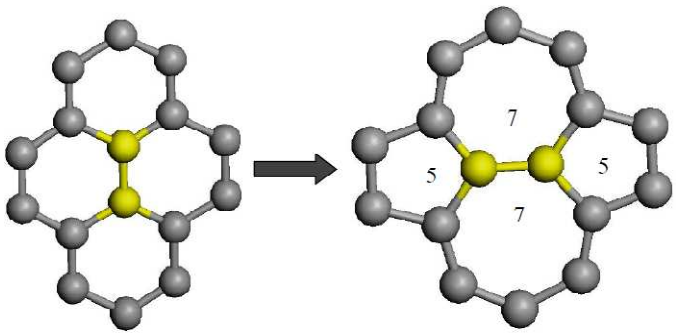

Fig. 5.1: Formation of a Stone-Wales defect through a 90° bond rotation.

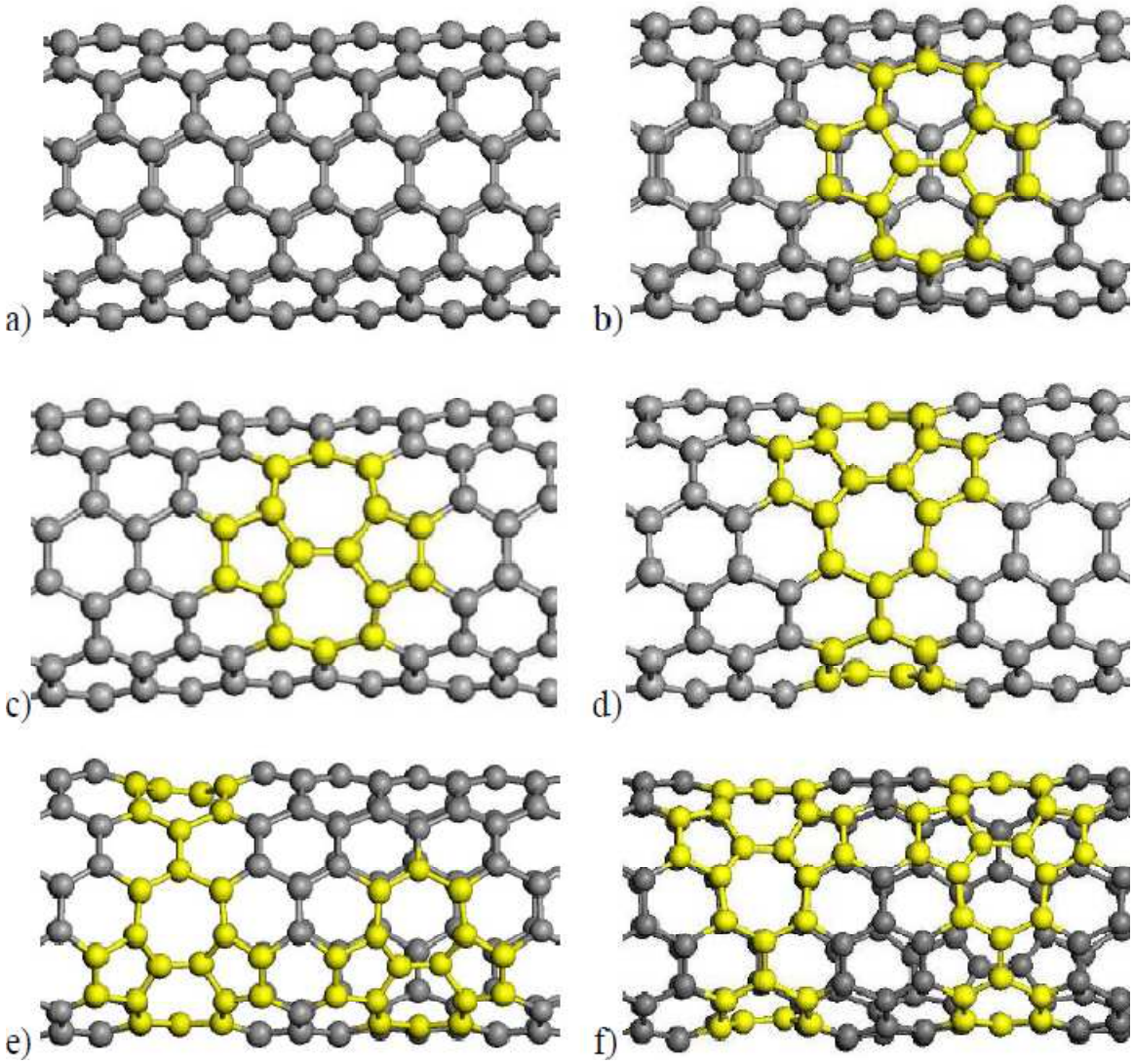

Fig. 5.2: SWCNT (6,6) with a) no defects (perfect) and b) 1, c) 2, d) 3, e) 4, and f) 5 Stone-Wales defects(Not in full scale).

5.1.2 Finite element modeling

In this section, we employ a molecular-continuum analogy to develop a 3-D atomistic finite element (FE) model using ANSYS® commercial FE software. To create the atomistic FE model, nodes are placed at the locations of carbon atoms in the CNT, and the covalent bonds between them are modeled using three-dimensional elastic beam elements with uniform circular cross-sectional areas.The resulting FE model is solved in two key steps: In the first step, the concept of energy equivalence is used to obtain the elastic properties (Young's modulus and shear modulus) and geometry (diameter and length) of the elastic beam elements. This data, in turn, serves as input to the FE code (described in Section 3.2), which is used to determine the force-deformation behavior of the atomistic CNT model in an in uniaxial tension test.

5.2 Molecular dynamics simulation

5.2.1 Molecular dynamics simulation of SWCNT

Molecular dynamics simulation runs of defective SWCNT with (6,6) chirality (Fig.5.1 and Fig. 5.2) was conducted at a temperature of 298K and a pressure of 1 atm for 50 pico-seconds (ps) with a time step of 1 femto-seconds (fs). In order to determine the mechanical properties, the nanotube was strained in the longitudinal direction and the internal stress of the cell was monitored which enabled the determination of the Young's modulus of the nanotubes (detail in section 4.2). All simulation analyses employed NPT ensemble using the parameters shown in Table 5.1.

Table 5.1: Parameters used in the molecular dynamics simulations.

MD Simulation Parameters	
MD ensemble	NPT
Duration of simulation	50ps
Time step	1 fs
Temperature	298 K

5.2.2 Molecular dynamics simulation of matrix

In the present study as a thermoplastic material polyethylene (PE) has been chosen as the matrix. Polyethylene is created through polymerization of ethane. The density of commercial PE is 0.8-1.0 g/cm^3. Depending on the density polyethylene is categorized as HDPE (high density polyethylene), MDPE (medium density polyethylene), LDPE (low density polyethylene) or VLDPE (very low density polyethylene).

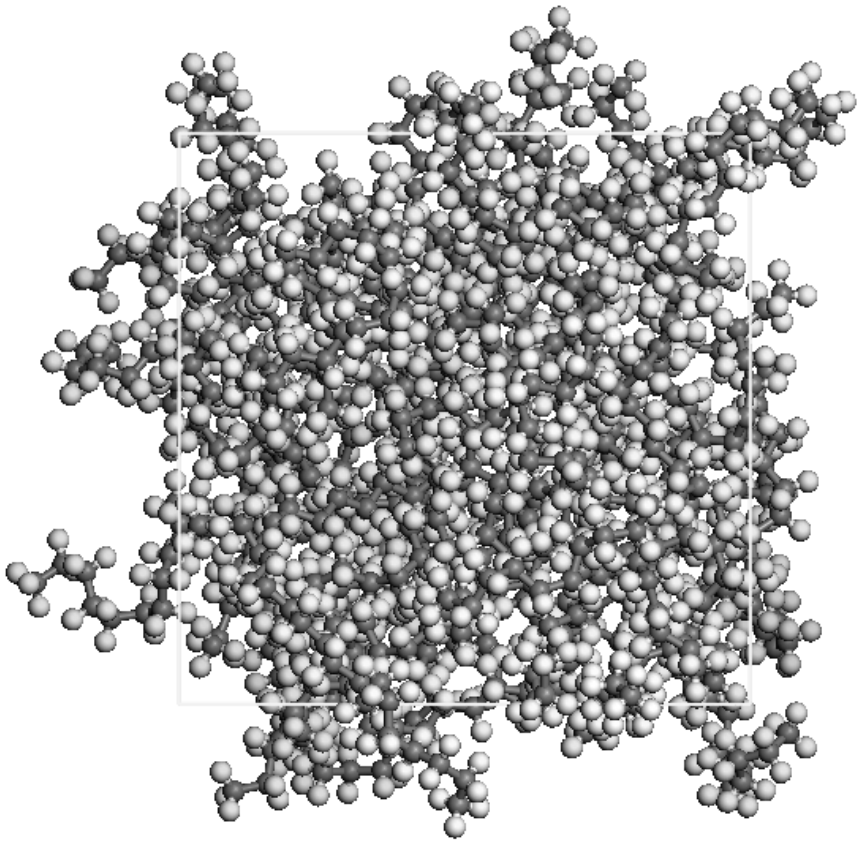

Fig. 5.3: Molecular Dynamics simulation cell of Polyethylene matrix.

In this study, the final density of the amorphous polyethylene was found to be 0.92g/cm^{3}and thus considered as LDPE. Molecular Simulation of the polyethylene matrix (Fig. 5.3) involves COMPASS [66] forcefield.

The first stage of dynamics was carried out for 50 ps with a time step of 0.5 fs under NVT ensemble and it was followed by NVE ensemble using the same time step but for a total time of 10 ps. The next stage was carried out under NPT ensemble for several thousand steps depending on the structure and it was followed by NVE ensemble in order to obtain a structure with minimum initial stress. All the simulations were carried out at 1 atm pressure and at a

temperature of 298 K. The final density of the amorphous polyethylene matrix was maintained at 0.92 g/cm^3.

5.2.3 Molecular dynamics simulation of the SWCNT–polymer composites

In case of SWCNT–polyethylene composites similar simulation procedure was followed as described earlier in section 5.2.2.

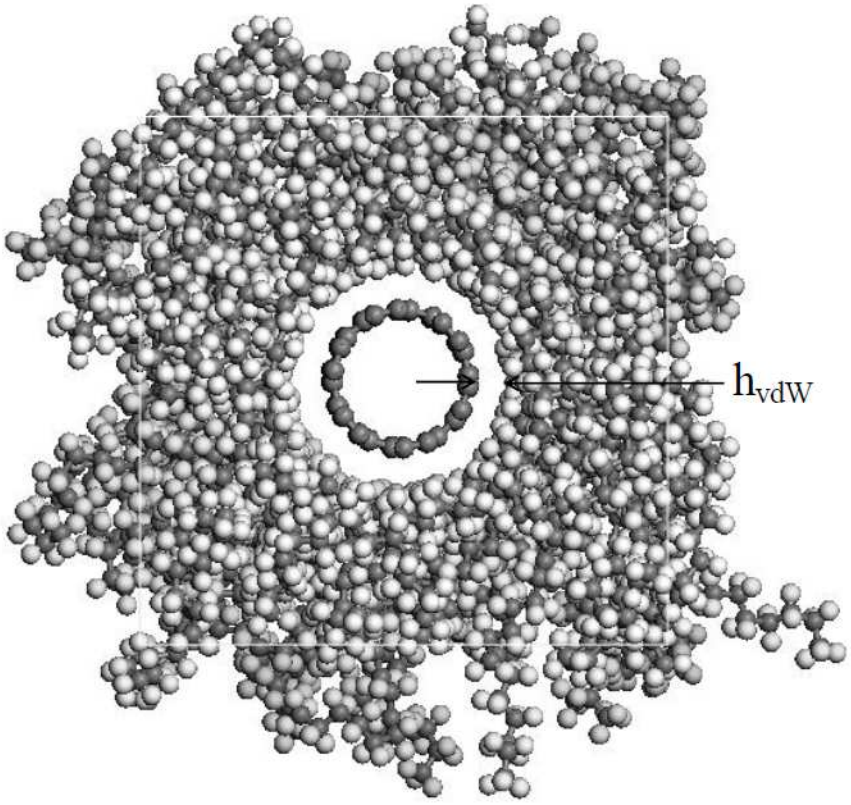

Fig. 5.4: Molecular Dynamics simulation cell of SWCNT-PE Composite (carbon and hydrogen atoms are colored as gray and white respectively).

For a composite system shown in Fig. 5.4 the dimensions of the simulation cell were maintained according to the data in Table 2. In order to investigate the effect of SW on a SWCNT-PE composite system, a total of 24 composite systems were modeled and simulated by varying the lattice parameters listed in Table 5.2.

Table 5.2: Lattice parameters of the simulation cell.

Composite System	A_{cell}(Å)	Volume Fractions (%)
I	23.25×23.25	16.1
II	25.0×25.0	14.0
III	27.0×27.0	12.0
IV	30.0×30.0	9.7

5.3 3-D finite element simulation

A 3-D atomistic FE model is developed in ANSYS®. In the atomistic FE model, the carbon nanotube is modeled as a frame-like structure, and the primary bonds between two nearest-neighboring atoms are modeled as elastic beam elements (i.e. ANSYS®BEAM4), as shown in Fig. 3.2. The elastic properties (Young's modulus and shear modulus) and geometry (length and diameter) of the beam elements were obtained in Sec. 3.2.1. As with the MD simulations, five different molecular systems of SWCNTs with chirality (4,4), (5,5), (6,6), (7,7), and (8,8), and Stone-Wales defects ranging from 0 to 5 for each structure, were modeled (Fig. 5.5).

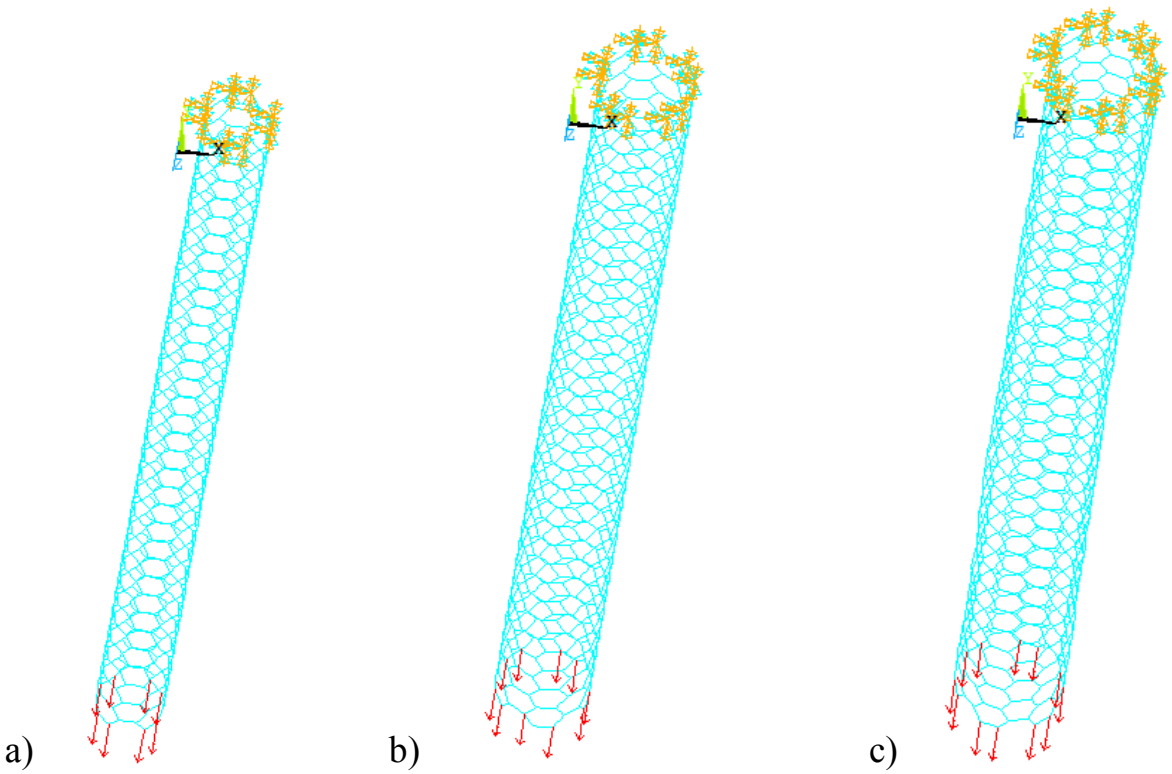

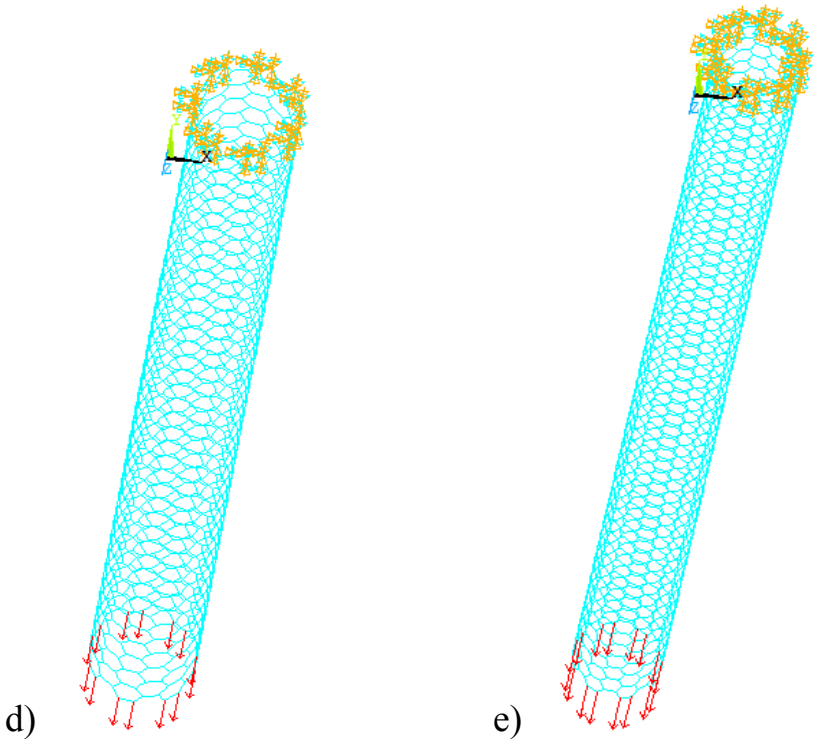

Fig. 5.5: Finite element models of a) (4,4), b) (5,5), c) (6,6), d) (7,7), and e) (8,8) SWCNTs. The far end of the nanotube is fixed, and the near end is subjected to a uniform tensile load.

To calculate the longitudinal Young's modulus of the SWCNTs, a uniaxial tension test was simulated. In the simulation, one end of the nanotube was fixed, and the other end was subjected to a uniform longitudinal tensile load F. By measuring the resulting longitudinal displacement ΔL of the SWCNT, the Young's modulus of the nanotube was determined using Hooke's law:

$$Y = \frac{\sigma}{\epsilon} = \frac{F/A}{\Delta L/L} = \frac{FL}{\pi D t_w \Delta L} \tag{5.1}$$

Where $A = \pi D t_w$ is the cross-sectional area of the CNT, D is the CNT diameter, t_w is the effective CNT wall thickness, and L is the initial length of the CNT.

Note that in Eqn. (5.1), the diameter D and length L are specified geometric parameters of the CNT, F is an input to the finite element simulation, and ΔL is an output of the finite element

simulation. Different values of the effective CNT wall thickness t_w, ranging from 0.64 to 6.9 Å, have been used in the literature (Table 5.3).

Table 5.3: Different values of CNT wall thickness used in the literature.

Authors	Method	Wall Thickness(Å)
[28]Kudin et al.	Ab initio computations	0.89
[49]Li and Chou	Structural mechanics:stiffness matrix method	3.4
[48]Odegard et al.	Equivalent-continuum modeling	6.9
[67]Yakobson et al.	Molecular dynamics	0.66
[68]Zhou et al.	Tight-binding model	0.74
[69]Tu and Ou-Yang	Local density approximation model	0.75
[70]Pantano et al.	Continuum shell modeling	0.75
[71]Hernandez et al.	Tight-binding molecular dynamics	3.4
[72]Jin and Yuan	Molecular dynamics	3.4
[73]Lu	Molecular dynamics	3.4

Fig. 5.6 shows the variation of Young's modulus (predicted by FE simulation) of CNT with tube wall thickness. It is clear from Fig. 5.6 that Young's modulus is strongly dependant on the tube wall thickness. As the tube wall thickness increases modulus value decreases significantly. MD simulation predicts the Young modulus as 1TPa. The same result for FE simulation is obtained at tube wall thickness of 3.4Å. Thus for our FE simulations, we employ an effective wall thickness of 3.4 Å, this value is used in all of our simulations, regardless of the number of Stone-Wales defects, as the Young's modulus vs. wall thickness curves are found to be relatively insensitive to the number of defects (see Fig. 5.7). This trends shown in this figure were also predicted by the finite-deformation continuum model of Gao and Li [74] and the equivalent-continuum model of Odegard et al. [48].

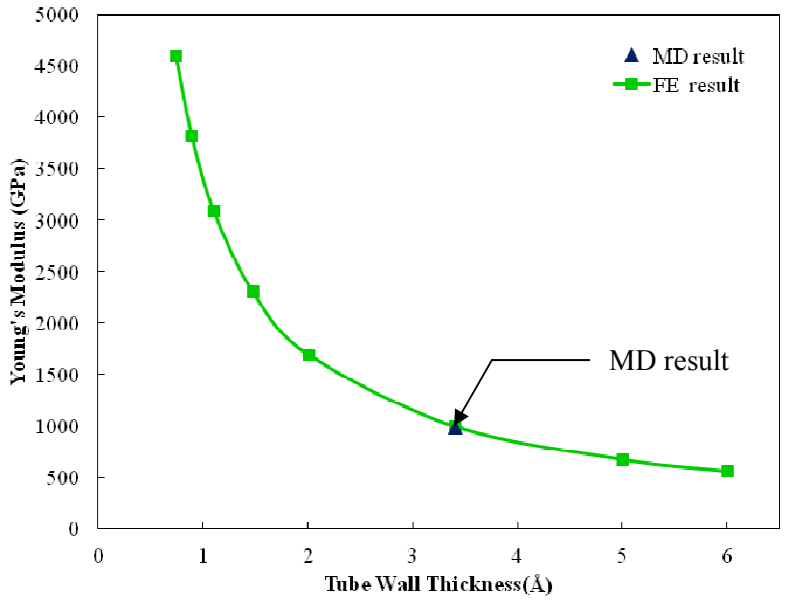

Fig. 5.6: Comparison of Young's moduli obtained from MD and FE simulations for different tube wall thicknesses (a perfect (6,6) CNT was used in the simulations). Agreement between the two methods occurs at a wall thickness of 3.4 Å.

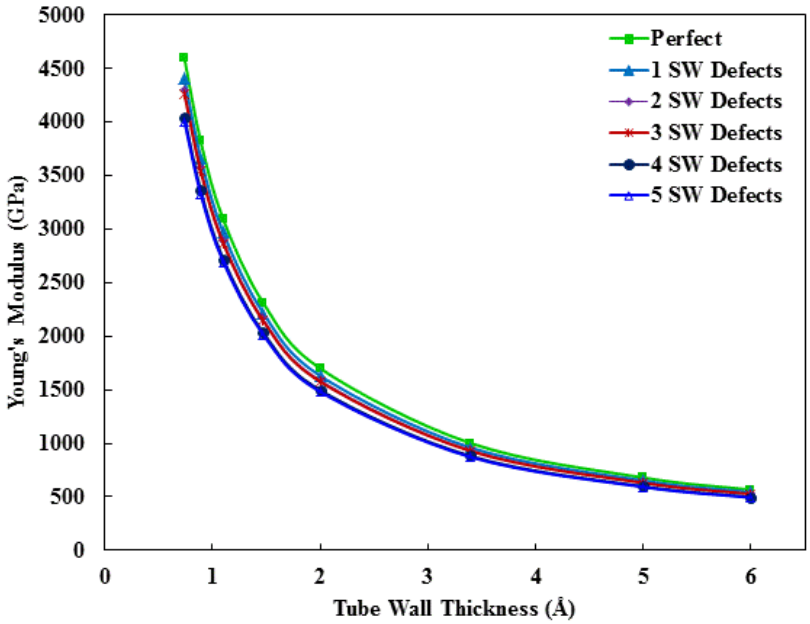

Fig. 5.7: Effect of tube wall thickness on the Young's modulus of SWCNT (6,6) with 0, 1, 2, 3, 4, and 5 Stone-Wales defects (obtained from FE analysis).

6. RESULTS AND DISCUSSION

6.1 Effect of position of the defects on Young's modulus of the nanotube

In the current research position of the SW defects on the Young's modulus of the carbon nanotube has been studied. SWs were formed at three different positions. The first type of SW was formed as mention in section 5.1.1.1 i.e both side and both direction (i.e longitudinal and radial) of the nanotube, second types of SW was formed in the longitudinal direction and at the same side of the nanotube, finally third types of SW was formed in random location of the nanotube. The effect of the three different positions of the SWs on the Young's modulus of the carbon nanotube (6,6) has been shown in Fig. 6.1.

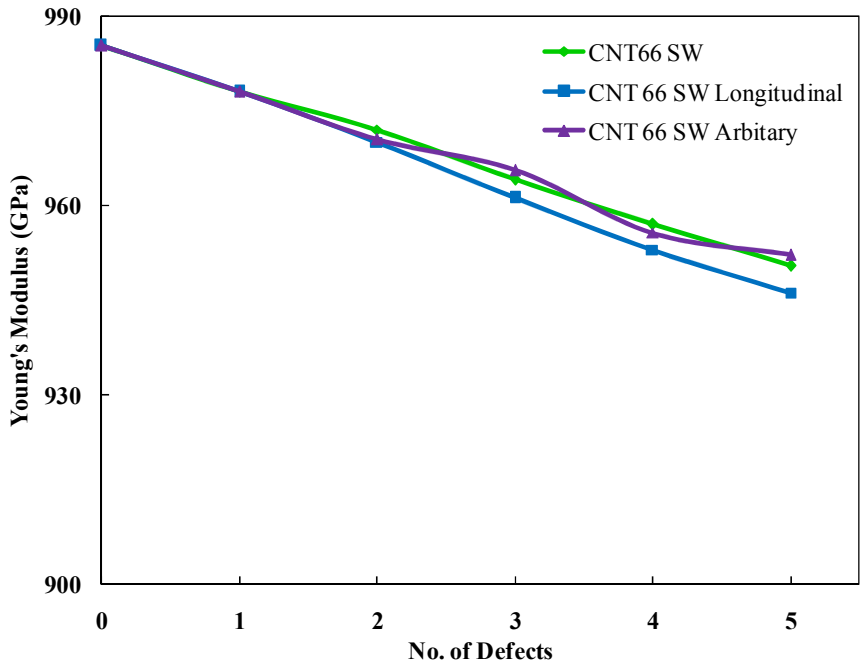

Fig. 6.1: Effect of position of the defects on the Young's modulus of SWCNT (6,6) with 0, 1, 2, 3, 4, and 5 Stone-Wales defects (obtained from MD simulation).

In Fig. 6.1 CNT66 SW indicates first types of defect, CNT66 SW longitudinal indicates second types of defects and CNT66 SW Arbitary indicates the third types of defects. In case of first types of defect (current research focus this type of defect throughout the paper) Young's modulus is slightly higher than second types of defect i.e longitudinal. Third type of defect gives Young's modulus that is very close to first types as shown in Fig. 6.1. But variation in Young's modulus between first and second types is less than 0.4% (0.004), and this variation between first and third types of defects reduces to 0.2% (0.002). Although position of the defects has effects

on Young's modulus of the nanotube but this is negligible. Considering three types of defects current research will focus only on the first types of defects and effect of the other types of defects can be predicted using the percentage variation determined in the current research using MD simulation.

6.2 Young's modulus of SWCNTs using MD simulations

6.2.1 Effect of nanotube diameter

The Young's moduli for the five chiral systems with 0, 1, 2, 3, 4, and 5 Stone-Wales defects are presented in Table 6.1.

Table 6.1: Longitudinal Young's modulus of SWCNTs obtained from MD and FE simulations.

No. of Stone-Wales Defects	Longitudinal Young's Modulus of SWCNTs (GPa)									
	(4,4)		(5,5)		(6,6)		(7,7)		(8,8)	
	MD	FE	MD	FE	MD	FE	MD	FE	MD	FE
0	976.4	956.4	982.5	991.7	985.2	1005.2	986.9	1026.1	988.0	1039.8
1	966.3	737.3	972.6	908.9	977.9	959.7	981.2	978.8	982.5	1003.1
2	957.8	564.9	966.3	797.3	972.4	917.2	976.0	943.1	978.1	967.0
3	948.9	493.0	957.2	768.9	964.6	875.7	969.0	912.4	972.0	952.0
4	940.0	483.7	947.7	757.3	957.6	858.7	963.3	906.6	967.1	939.3
5	925.9	480.7	938.6	735.9	950.4	840.9	959.1	898.9	963.3	928.2

A comparison in Fig. 6.2 reveals that the Young's modulus of both pristine and defective SWCNTs increases with nanotube diameter. In Fig. 6.3, a plateau modulus is reached for diameters greater than 9.5Åfor all tubes, irrespective of the number of defects. The magnitude of this plateau modulus increases as the number of defects decreases.

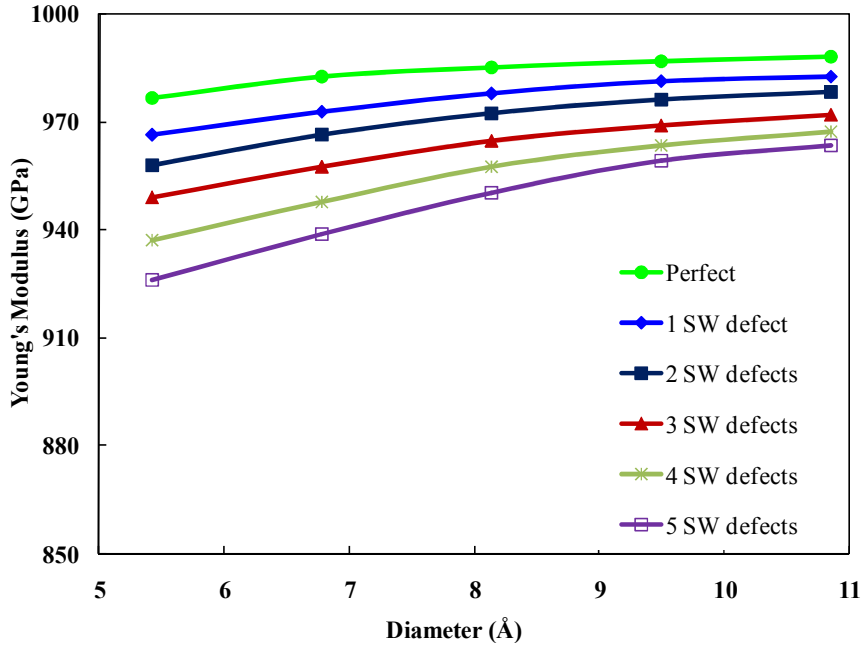

Fig. 6.2: Effect of nanotube diameter on the Young's modulus of defective CNTs (obtained from MD simulations).

For diameters less than 9.5Å, the modulus decreases from the associated plateau level due to increased curvature strain. This result is physically intuitive: as the curvature strain is increased, the C-C bonds are weakened, and this effect should be reflected in the mechanical properties.

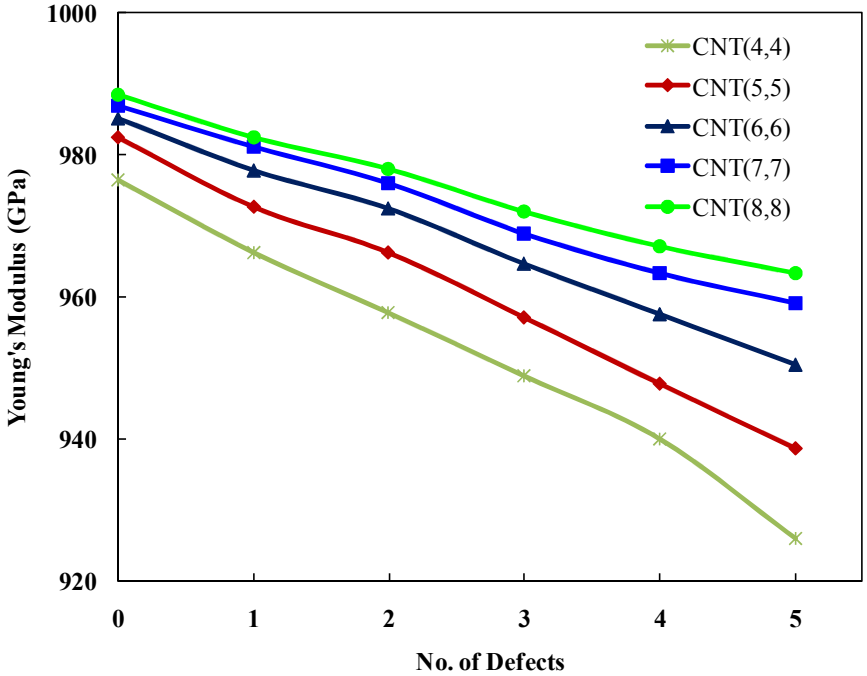

Fig. 6.3: Effect of the number of Stone-Wales defects on the Young's modulus of different CNT structures (obtained from MD simulations).

6.2.2 Effect of Stone-Wales defects

It is clear from Fig. 6.3 that as the number of Stone-Wales defects increases, the Young's modulus of the single-walled carbon nanotubes decreases. For larger-diameter SWCNTs, the effect of the Stone-Wales defects is less significant than smaller-diameter SWCNTs. For example, in case of a (4,4) SWCNT, the Young's modulus decreases by nearly 50GPa, or about 5.1%, as the number of SW defects is increased from 0 to 5. In contrast, for the case of a (8,8) SWCNT (two times larger in diameter than a (4,4) SWCNT), the Young's modulus decreases only 24.5 GPa, or about 2.5%, as the number of SW defects is increased from 0 to 5.

6.3 Young's modulus of SWCNTs using FE simulations

6.3.1 Effect of nanotube diameter

Table 6.1 shows the Young's moduli predicted by our FE simulations for the five chiral systems with 0, 1, 2, 3, 4, and 5 Stone-Wales defects.

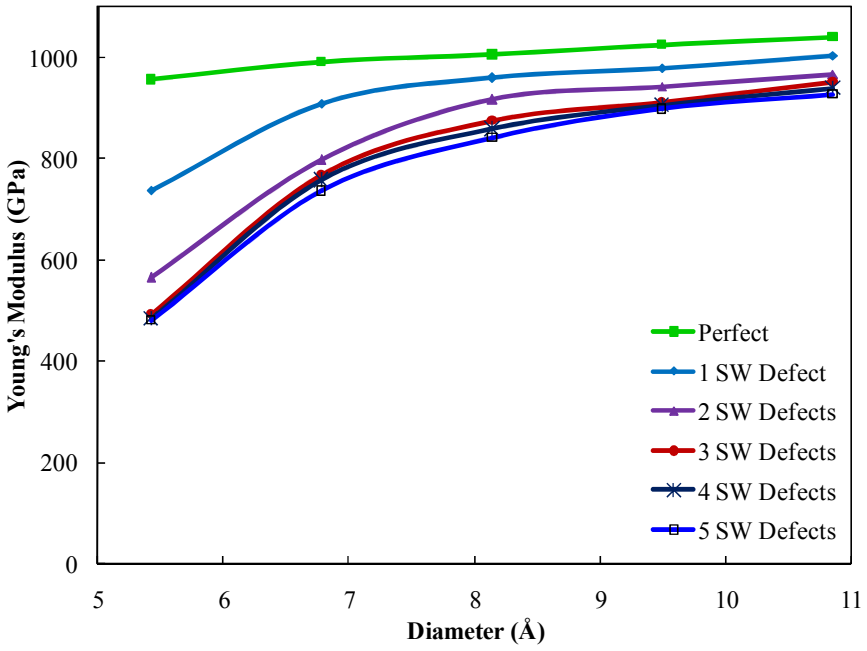

Fig. 6.4: Effect of nanotube diameter on the Young's modulus of defective CNTs (obtained from FE analysis, t=3.4Å).

It is clear from Fig. 6.4 that as the nanotube diameter increases, Young's modulus also increases, although at a decreasing rate. This trend is observed for both pristine and defective SWCNTs, although the increase is more pronounced for defective SWCNTs at small diameters. Figure 13

reveals that a plateau modulus is reached for tube diameters greater than 9.5 Å, irrespective of the number of defects.

6.3.2 Effect of Stone-Wales defects

Fig. 6.5 shows the effect of the number of Stone-Wales defects on the Young's modulus of the SWCNTs. As the number of Stone-Wales defects increases, the modulus of the single-walled carbon nanotubes decreases, although at a decreasing rate. For smaller-diameter SWCNTs, the effect of Stone-Wales defects is more significant than larger-diameter SWCNTs.

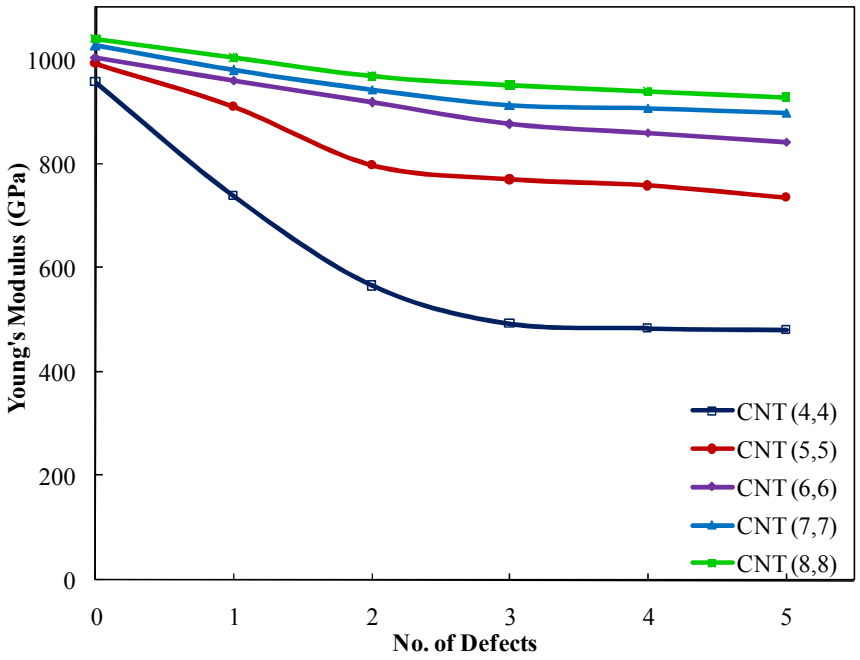

Fig. 6.5: Effect of the number of Stone-Wales defects on the Young's modulus of different CNT structures (obtained from FE analysis, t=3.4Å).

As an example, the (4,4) SWCNT experiences a nearly 50% decrease in Young's modulus as the number of SW defects is increased from 0 to 5, whereas the (8,8) SWCNT (two times larger in diameter than a (4,4) SWCNT) only experiences a 10% decrease in Young's modulus over the same range.

6.4 Comparison of MD and FE results

The Young's moduli predicted by our MD and atomistic FE analyses are shown in Table 6.1. The highest moduli are observed in larger-diameter defect-free CNTs, while the lowest moduli are observed in smaller-diameter defective CNTs.

The less computationally expensive atomistic FE approach captures several key trends in concert with the MD approach: Stone-Wales defects tend to degrade the tensile modulus of CNTs (Fig. 6.3 and Fig. 6.5), larger-diameter CNTs exhibit a higher tensile modulus (Figures 6.2 and 6.4), and larger-diameter CNTs are less sensitive to the presence of additional defects (Fig. 6.2 and Fig. 6.4).However, Fig. 6.6 to Fig. 6.7 indicate that the atomistic FE approach consistently underpredicts the Young's modulus. The degree to which FE underpredicts is dependent on the number of defects and the CNT diameter.

Fig. 6.6 and Fig. 6.7 indicate that the agreement between the FE and MD results diminishes substantially as the number of defects increases from 0 to 2. Beyond 2 defects, however, the FE-predicted tensile modulus becomes less sensitive to the presence of additional defects, and the disparity between the FE and MD results steadies.

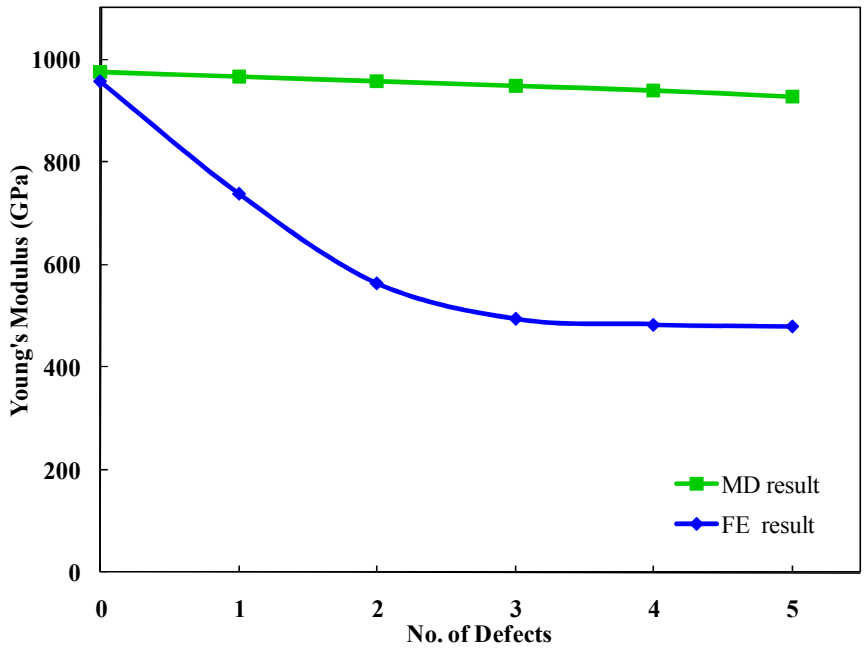

Fig. 6.6: Comparison of Young's modulus vs. number of Stone-Wales defects from MD and FE simulations for SWCNT (4,4) (for FE analysis, t=3.4Å).

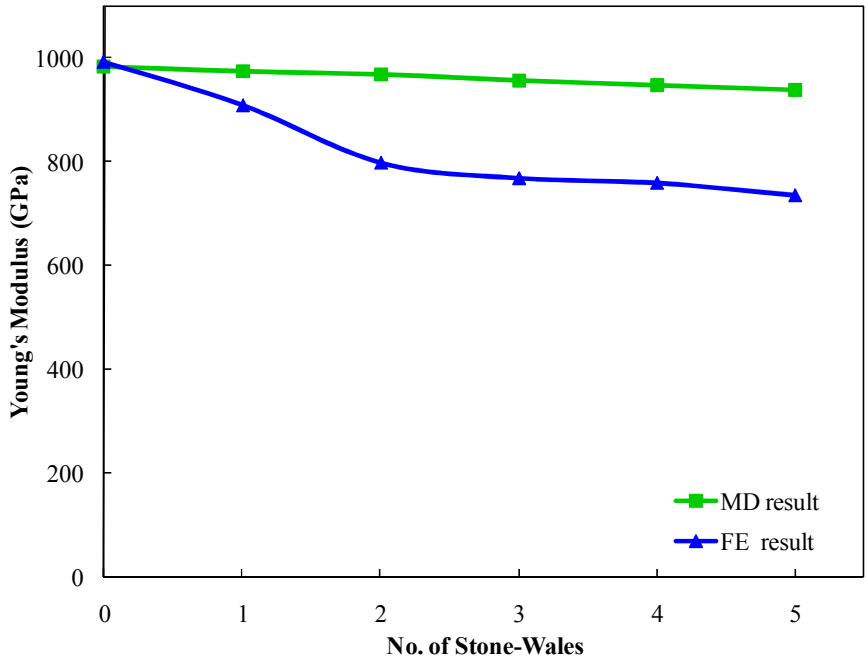

Fig. 6.7: Comparison of Young's modulus vs. number of Stone-Wales defects from MD and FE simulations for SWCNT (5,5) (for FE analysis, t=3.4Å).

The degree to which FE underpredicts the tensile modulus is less pronounced for the larger-diameter (5,5) CNT than the smaller-diameter (4,4) CNT. A similar pattern was reported by Lu [16] for atomistic FE simulations of SW defects at random locations in the CNT. Lu showed that the stiffness and strength may not decrease monotonically with increasing number of defects. This observation is further confirmed by Fig. 6.8, which shows good agreement in the percent reduction in tensile modulus for defective CNTs with diameters larger than 9.5Å, and substantially worse agreement for defective CNTs with diameters smaller than 7Å. CNT tensile moduli results reported in the literature are listed Table 6.2 for a comparison with the current study.

Table 6.2: Young's moduli of CNTs obtained by different methods in the literature.

Authors	Method	Young's Modulus (TPa)
[29]Lier et al.	*Ab initio*	0.72-1.120
[72]Lu	Empirical force constant model	0.971-0.975
[75]Yao and Lordi	Molecular dynamics	1.0
[76]Salvetat et al.	Experimental(atomic force microscope)	1.0
[77]Demczyk et al.	Experimental (pull and bend test)	0.91
[78]Yu et al.	Experimentaltension test	0.32-1.47
Present study	Molecular dynamics	0.926-0.988
	Finite element analysis	0.481-1.0398

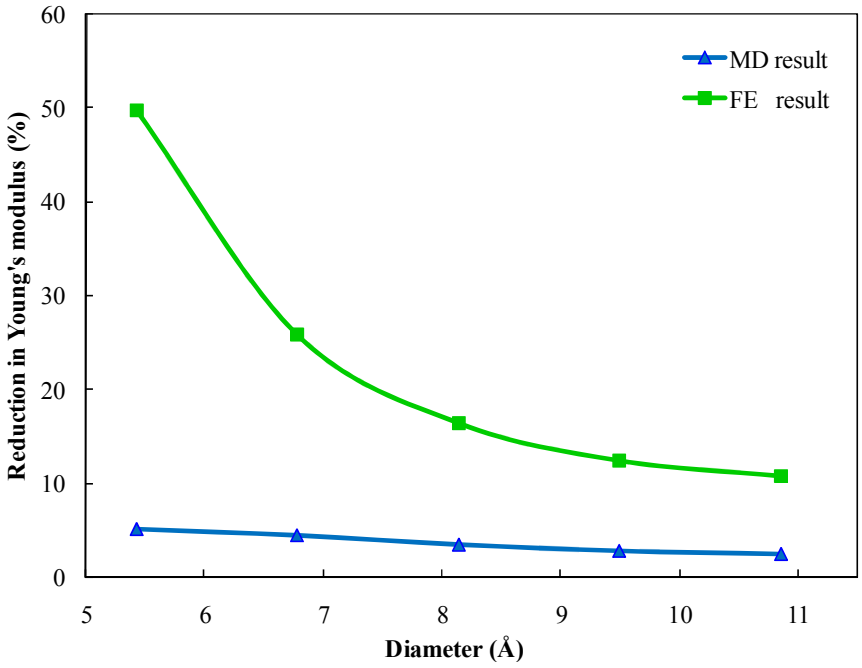

Fig. 6.8: Comparison of MD and FE results quantifying the reduction in Young's modulus with increasing tube diameter (for a CNT with 5 Stone-Wales defects relative to a pristine CNT).

6.5 Elastic properties of polyethylene

The matrix material of the nanocomposite in the current study is pure polyethylene. However, pure amorphous polyethylene is not available in reality, so it is not possible to verify the simulated results with experiments. Commercially available polyethylene is semi-crystalline and exists in various categories as mentioned in section 5.2.2.

Table 6.3: Properties of polyethylene matrix obtained from MD simulation.

Polyethylene Matrix		
Density(g/cc)	Young's Modulus(GPa)	Poisson's Ratio
0.92	1.005	0.37

Young's modulus and Poisson's ratio of the amorphous polyethylene matrix found from our simulation are 1.005 GPa and 0.37 respectively (Table 6.3). Elastic modulus of commercially available LDPE lies between 0.262 and 0.869 GPa [79], which is consistent with our simulated result. The slight discrepancy in the modulus is most likely caused by the presence of defects in the molecular structure of the actual amorphous polyethylene.

6.6 Elastic properties of SWCNT-PE nano composites

MD simulation was conducted for four different volume fractions of the nanocomposites and the corresponding volume fractions, calculated using Eq. (4.3) are listed in Table 5.2. The Van-der-Waals separation distance (h_{vdW}) was calculated from radial distribution function (RDF) obtained from the simulation. The RDF is zero within the vdW separation distance as there are no atoms within this region. It should be noted that due to their regular atom packing for each individual unit cell, the vdW separation distance could be slightly different for the unit cells containing the same matrix and the same SWCNT. Average vdW separation distance used in the current simulation was 2.40 Å.

The effect of the number of SW defects in CNTs on the Young's modulus composite at various volume fractions is shown Fig. 6.9.

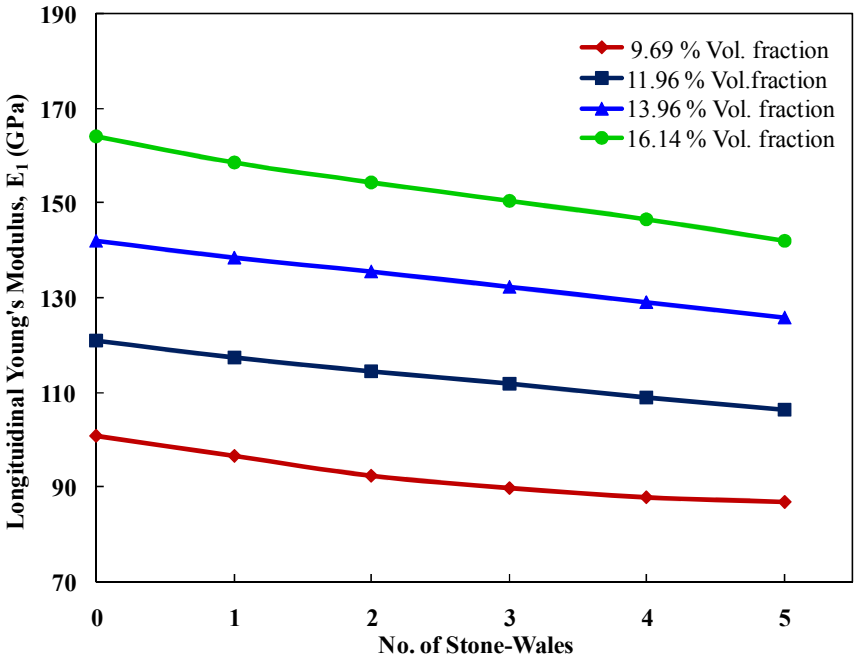

Fig. 6.9: Effect of the number of Stone-Wales defects in CNTs on the overall Young's modulus of SWCNT-PE nanocomposite.

Similar to the case of an individual CNT, the composites exhibit an approximately linear pattern of decrease in Young's modulus with increasing number of SW defects. The highest Young's modulus of 164.3 GPa is obtained for composites of perfect SWCNTs at a volume fraction 16.1%. The lowest Young's modulus of 86.4 GPa is found for composites of CNTs with 5 SW defects at a volume fraction 9.7%. A slight disparity in the slopes of the different volume fraction curves can be noted in Fig. 6.9. The number of SW defects in CNTs have a greater impact on the overall Young's modulus of the composites with greater CNT concentrations (i.e. volume fractions), indicating that, for higher volume fractions, properties of the SWCNT dominates the properties of the nanocomposites.

As expected, the Young's modulus of the composite is strongly dependent on volume fractions of the SWCNTs. The longitudinal Young's modulus of the nanocomposites linearly increases with higher volume fractions of CNTs in the composite (Fig. 6.10). Furthermore, a diverging trend of the curves is observed towards volume fractions higher than 13%, indicating the increased dominance of CNT properties beyond this region.

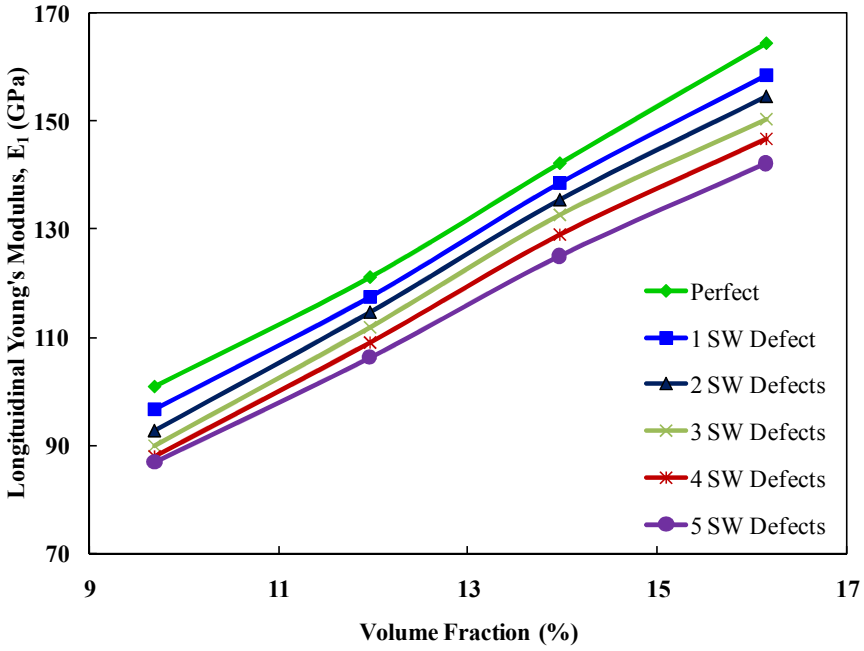

Fig. 6.10: Effect of Volume fraction on Young's modulus of SWCNT-PE nanocomposites based on MD simulations. An increase in the number of SW defects in the CNTs results in lower values of the overall modulus for a given volume fraction.

For comparison, the effect of volume fraction on Young's modulus of SWCNT-PE nanocomposites obtained from the rule of mixtures theory is shown in Fig. 6.11. A careful observation shows the divergence of the curves as one moves toward higher volume fraction, indicating that the effect of the number of SW defects becomes dominant at greater concentration of CNT reinforcements. Variation of longitudinal Young's modulus between perfect and 5 number of SW defective SWCNT-PE nanocomposites is shown in Fig. 6.12, where ΔE_1denotes the difference of longitudinal Young's modulus between composites with pristine and with 5 SW defects CNTs.

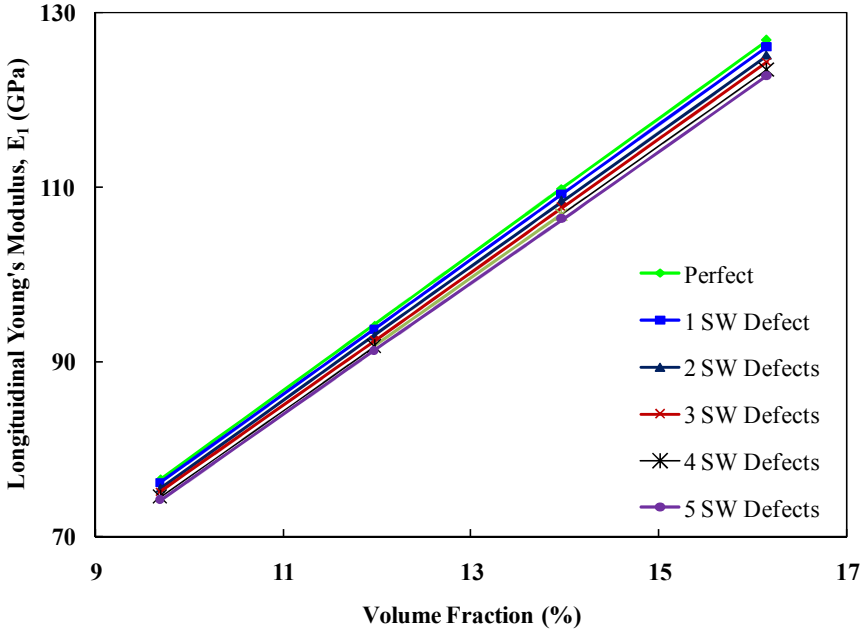

Fig. 6.11: Effect of Volume fraction on Young's modulus of SWCNT-PE nano composite as computed with rule of mixture. Although the modulus increases monotonically for all cases, the effect of the number of SW defects on Young's modulus is more significant at higher volume fraction of CNTs.

It is clear from this figure that for volume fractions<13%, the effect of SWs is less significant but for higher volume fractions (Vf>13%) SW defects play an important role on the longitudinal Young's modulus. Since Fig. 6.10 and Fig. 6.11 report the Young's modulus of nanocomposites using MD simulation and RM separately, we combine representative curves from each figure for closer comparison in Fig. 6.13.

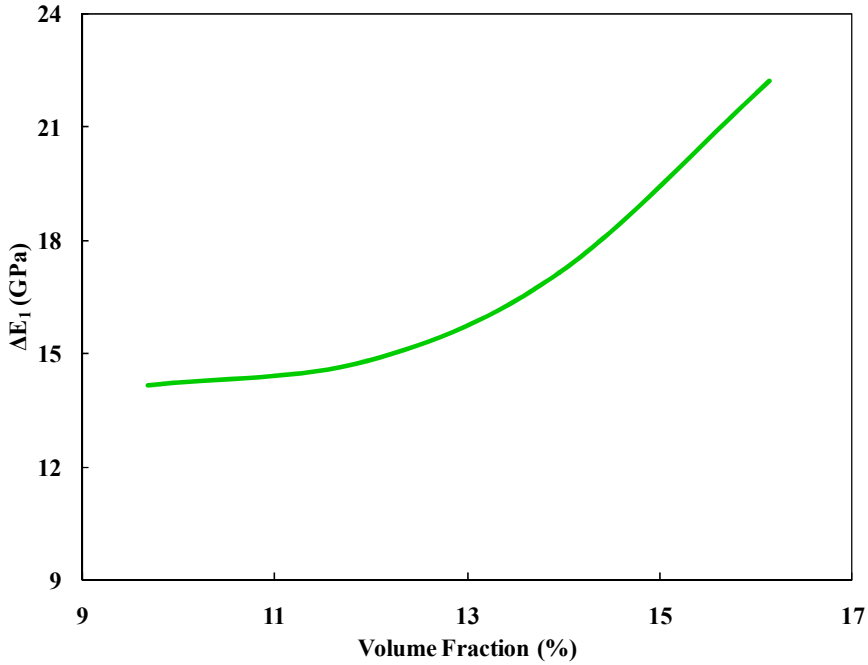

Fig. 6.12: Effect of CNT volume fraction on the longitudinal Young's Modulus of a composite shown as the difference between composites with pristine and with 5 SW defects CNTs.

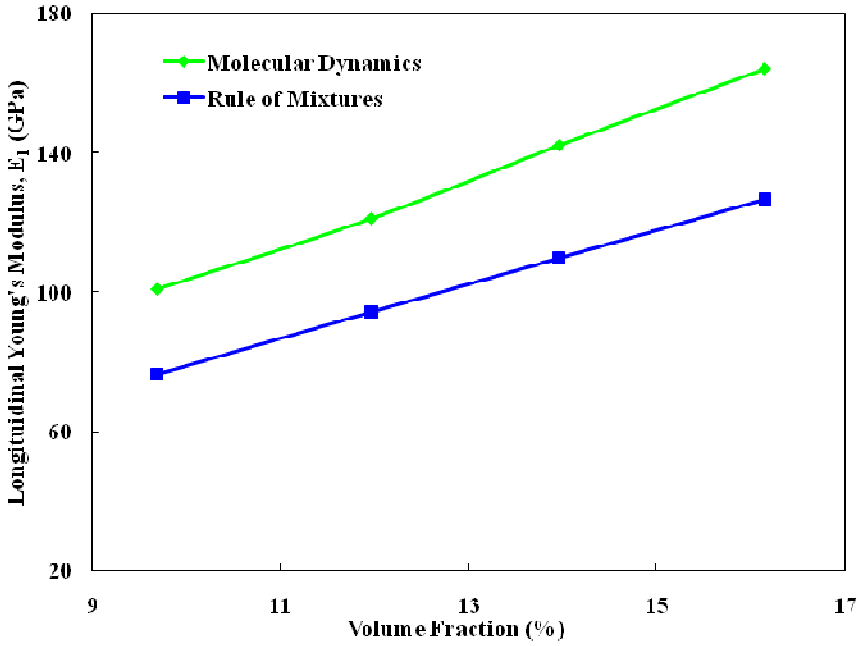

Fig. 6.13: A Comparison of longitudinal Young's moduli obtained from MD simulation and Rule of Mixtures for composites with pristine SWCNTs.

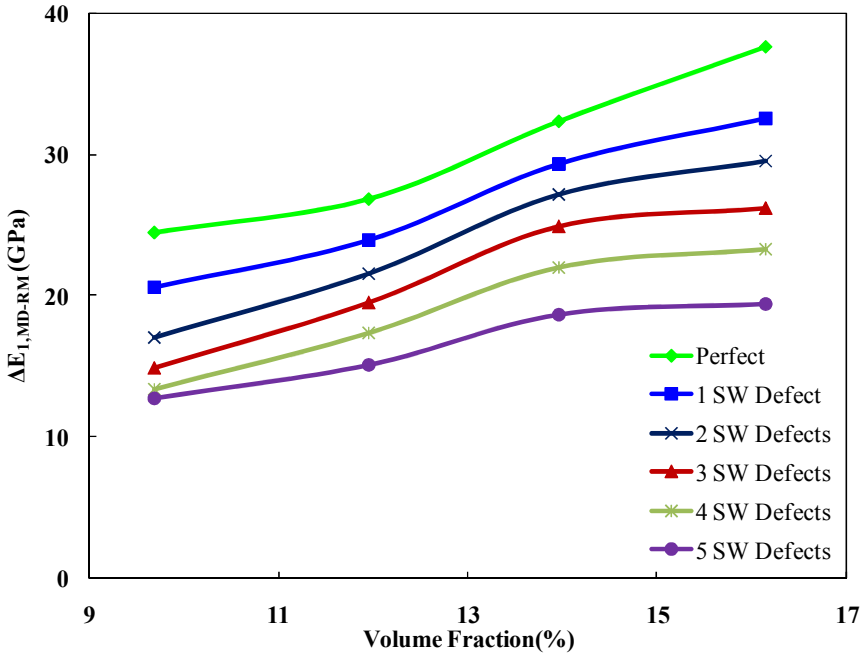

Fig. 6.14: A Comparison of the difference in longitudinal Young's modulus between MD and RM results. The difference increases with the volume content of CNT. However the difference is decreased as the number of Stone Wales defects increases in a single CNT.

Although both methods predict a linear increase in modulus with increasing volume fractions of nanotubes, MD simulation predictions are consistently higher compared to RM results. Fig. 6.14 represents a comparison of difference in longitudinal Young's modulus between MD and RM results for all the molecular models, where $\Delta E_{1,\,MD\text{-}RM}$ is the difference of longitudinal Young's modulus between MD and RM results. Accuracy of RM results is found to decrease with increase in CNT volume fraction.

7. CONCLUSION

Motivated by a significant variation in the Young's moduli appearing in the CNT literature, the effect of Stone-Wales defects on the tensile modulus of single-walled carbon nanotubes with different chiralities was investigated using MD simulations and FE analysis. Both MD and FE calculations show good agreement in the case of all pristine SWCNTs. However, the accuracy of the FE results decline for defective nanotubes with diameters less than 9.5Å. Stone-Wales defects reduce the Young's modulus of CNTs by approximately 2 to 5% for MD simulation and 10%-50% for FE analysis as the number of defects increases from zero to five.

In the present work mechanical properties of CNT composites with amorphous polyethylene matrix have been studied. In particular the effect of Stone-Wales (SW) defects on Young's modulus of amorphous polyethylene matrix reinforced with the (6,6) SWCNT have been investigated through molecular dynamics simulations. Our investigation shows that Young's modulus of the SWCNT is dependent on the number of SW defects; as the SW increases Young's modulus of the SWCNT decreases. Mechanical properties of the amorphous polyethylene obtained from the MD simulation are in good agreement with commercially available polyethylene. In case of SWCNT-PE nanocomposite, as the number of SW increases the longitudinal Young's modulus of the nanocomposite decreases. Longitudinal Young's modulus of the nanocompositeis strongly dependent on the number of SW defects in the CNTs for higher volume fractions ($V_f > 13\%$). A comparison between MD and RM has been made which show that MD simulation predict higher modulus than RM for all CNTs, both pristine and defective. Longitudinal Young's modulus difference between perfect and 5 SWs defective nanocomposite are much higher in case of higher volume fractions ($V_f > 13\%$) than for composites with lower volume fractions.

REFERENCE:

[1] Kroto H. W., Heath J.R, O'Brien S.C, Curl R.F, and Smalley R.E, , "C60 Buckyminster fullerence", Nature, vol. 318, pp. 162, (1985).

[2] Iijima S., and Icihashi T., "Single-shell carbon nanotubes of 1-nm diameter", Nature, vol. 363, pp. 603, (1993).

[3] Bethune D. S., Kiang C. H., Devries Gorman M.S.G., Savoy R., Vazquez J., and R. Beyers, "Cobalt-catalyzed growth of carbon nanotubes with single atomic layer walls", Nature, vol. 363, pp. 605,(1993).

[4] Treacy M. M. J., Ebbesen T. W., and Gibson T. M., "Exceptionally high Young's modulus observed for individual nanotubes", Nature, 381, pp. 678 (1996).

[5] Wong E. W., Sheehan P. E, and Lieber C. M., "Nanobeam mechanics: Elasticity, strength, and toughness of nanorods and nanotubes", Science, vol. 277, pp. 1971 (1997).

[6] Dujardin E., Webbesen T. W., Krishan A., ianilos P. N., and Trecy M. M. J., "Young's Modulus of Single-Walled Nanotubes", Physical Review B, vol. 58, pp. 14013 (1998).

[7] Falvo M. R., Clary G. J., Taylor R. M., Chi V., Brooks F. P., and Washburn S., "Bending and buckling of carbon nanotubes under large strain", Nature, vol. 389, pp.582 (1997).

[8] Bower C., Rosen R., Jin L., Han J., and Zhou O., "Deformation of carbon nanotubes in nanotube– polymer composites",Applied Physics Letters, vol. 74, pp. 3317 (1999).

[9] Iijima S., Brabec C., Maiti A., and Bernholc J., "Structural flexibility of carbon nanotubes", Journal of Chemical Physics, vol. 104, pp. 2089(1996).

[10] Dekker C., "Carbon nanotubes as molecular quantum wires",Physics Today, vol. 52, pp. 22 (1999).

[11] Ebbesenand T. W., and Takada T., "Topological and SP^3 defect structures in nanotubes", Carbon, vol. 33, pp. 973(1995).

[12] Sammalkorpi M., Krasheninnikov A., Kuronen A., Nordlund K. and Kaski K., “Mechanical properties of carbon nanotubes with vacancies and related defects”, Phys. Rev. B, vol. 70, pp. 245(2004).

[13] Lu Q. and Bhattacharya B., “Effect of randomly occurring Stone–Wales defects on mechanical properties of carbon nanotubes using atomistic simulation”, Nanotechnology, vol. 16, pp. 555(2005).

[14] Feynman R. P., “There's plenty of room at the bottom [datastorage]”, Journal of Microelectro-mechanical Systems,, vol. 1, pp. 60, (1992).

[15] Binnig G., Rohrer H., Gerber C., and Weibel E., “Surface studies by scanning tunneling microscopy," Phys. Rev. Lett., vol. 49, pp. 57, (1982).

[16] Binnig G., Quate C. F., and Gerber C., “Atomic force microscope”, Phys. Rev. Lett., vol. 56, pp. 930, (1986).

[17] Nobelprize.org, “Nobel lectures in chemistry 1996-2000”, http://www.nobelprize.org. (2012).

[18] Kiang C.H., Endo M., Ajayan P. M., Dresselhaus G. and Dresselhaus M.S., “Size effects in carbon nanotubes”, Phys. Rev. Lett.,vol. 81, pp. 1869(1998).

[19] Krasheninnikov A. V., Nordlund K., and Keinonen J., “Production of defects in supported carbon nanotubes under ion irradiation”, Phys. Rev. B, 65, pp. 165423 (2002).

[20] Ajayan P. M., Ravikumar V., and Charlier J. C., “Surface Reconstructions and DimensionalChanges in Single-Walled Carbon Nanotubes”, Phys. Rev. Lett., vol. 81, pp. 1437 (1998).

[21] A. Lherbier, S. M.-M. Dubois, X. Declerck, S. Roche, Y. M. Niquet, and J. C. Charlier, "Two-Dimensional Graphene with Structural Defects: Elastic Mean Free Path, Minimum Conductivity, and Anderson Transition", Phys. Rev. Lett., vol. 106, pp. 046803 (2011).

[22] Kotakoski J., Meyer J. C., Kurasch S., Santos-Cottin D., Kaiser U., and Krasheninnikov A. V., "Stone-Wales-type transformations in carbon nanostructures driven by electron irradiation", Phys. Rev. B 83, 245420 (2011).

[23] M. B. Nardelli, B. I. Yakobson, and J. Bernholc, "Mechanism of strain release in carbon nanotubes", Phys. Rev. B, vol. 57, 4277–4280 (1998)

[24] Tang C., Guo W., and Chen C., "Nonlocal elasticity based magnetic field affected vibration response of double single-walled carbon nanotube systems", Phys. Rev. B, vol. 79, pp. 155436(2009).

[25] Huang Y., Wu J., and wang K. C. H., "Thickness of graphene and single-wall carbon nanotubes", Phys. Rev. B, vol. 74, pp. 245413 (2006).

[26] Pine P., Yaish Y. E., and Adler J., "Simulation and vibrational analysis of thermal oscillations of single-walled carbon nanotubes", Phys. Rev. B, vol. 83, pp. 155410 (2011).

[27] Sánchez-Portal D., Artacho E., Soler J. M., Rubio A.,and Ordejón P., "Ab-initio structural, elastic, and vibrational properties of carbon nanotubes", Phys. Rev. B, vol. 59, pp. 12678(1999).

[28] Kudin K. N. Scuseria G. E., and Yakobson B. I., "C_2F, BN, and C nanoshell elasticity from ab initio computations", Phys. Rev. B, vol. 64, pp. 235406 (2001).

[29] Lier G. V., Alsenoy C. V., VanDoren V., and Geerlings P. "Ab initio study of the elastic properties of single-walled carbon nanotubes and grapheme", Chem. Phys. Lett. Vol. 326, pp. 181(2000).

[30] Deng C. F., Wang D. Z., Zhang X. X. and Li A. B., "Graphene–aluminum nanocomposites", Mater.Sci. Eng. A, vol. 444, pp. 138(2007).

[31] Yoon P. J., Fornesand T. D., and Paul D.R., "Thermal expansion behavior of nylon 6 nanocomposites", Polymer, vol. 43, pp. 6727(2002).

[32] Zhu R., Pan E. and Roy A. K., "Molecular dynamics study of the stress-strain behavior of carbon-nanotube reinforced Epon 862 composites",Mater. Sci. Eng.A, vol. 447, pp. 51 (2007).

[33] Gou J., Minaie B., Wang B., Liang Z., and Zhang C.,"Computational and experimental study of interfacial bonding of single walleed nanotube reinforced composites", Comput. Mater.Sci. vol. 31, pp. 225 (2004).

[34] Li Z., Wang C. Y., Ke S. H. and Yang W., "First-principles study for transport properties of defective carbon nanotubes with oxygen adsorption", The Euro. Phys. J. B, vol. 69, pp. 375(2009).

[35] Yue H. and Elliot J., "Molecular dynamics simulations of the elastic properties of polymer/carbon nanotube composites", Comput. Mater.Sci., vol. 39, pp. 315(2007).

[36] Qian D., Dickey E. C., Andrews R. and Rantell T., "Load transfer and deformation mechanisms in carbon nanotube-polystyrene composites", Appl. Phys. Lett., vol. 76, pp. 2868(2000).

[37] Sen R., Zhao B., Perea D., Iktis M. E., Hu H., Love J., Bekyarova E. and Haddon R. C.,"Preparation of Single-Walled Carbon Nanotube Reinforced Polystyrene and Polyurethane Nanofibers and Membranes by Electrospinning", Nano Lett., vol. 4, pp. 459 (2004).

[38] Li X. D., Gao H. S., Scrivens W. A., Fei D. L., Xu X. Y., Sutton M. A., Reynolds A. P. and Myrick M. L., "Nanomechanical characterization of single-walled carbon nanotube reinforced epoxy composites", Nanotechnology, vol. 15, pp. 1416(2004).

[39] Frankland S. J. V., Harik V. M., Odegard G. M., Brenner D. W. and Gates T. S., "The stress–strain behavior of polymer–nanotube composites from molecular dynamics simulation", Comp. Sci. Tech., vol. 63, pp. 1655(2003).

[40] Frankland S. J. V., Caglar A., Brenner D. W. and Griebel M. J., "Molecular Simulation of the Influence of Chemical Cross-Links on the Shear Strength of Carbon Nanotube-Polymer Interfaces", Phys. Chem. B 106,3046(2002).

[41] Lei Z. K., Qiu W., Li Q., Kang Y. H. and Pan X. M., "Mechanical Properties of Carbon Nanotube Polymer Composites", Polym. Mater.Sci. Eng., vol. 12, pp.134(2008).

[42] Dalton A. B., Ferraris J.P., and Baughman R. H., "Continuous carbon nanotube composite fibers: properties, potential applications, and problems", J. Mater. Chem, vol. 14, pp. 1(2004).

[43] Gojny F. H., Nastalczyk J., Roslaniec Z., and Schulte K., "Surface modified multi-walled carbon nanotubes in CNT/epoxy-composites ", Chem. Phys. Lett., vol. 370, pp. 820(2003).

[44] Gojny F.H. and Schulte K., "Influence of different nanotube on mechanical properties of epoxy matrix composites", Compos.Sci. Technol., vol. 64, pp. 2303(2004).

[45] Nardelli M. B., Fattebert J. L., Orlikowski D., Roland C., Zhao Q., and Bernholc J., "Mechanical properties, defects and electronic behavior of carbon nanotubes", Carbon, vol. 38, 1703(2000).

[46] Chandra N., Namilae S., and Shet C., "Local elastic properties of carbon nanotubes in the presence of Stone-Wales defects", Phys. Rev. B, vol. 69, pp. 094101 (2004).

[47] Liew K. M., He X. Q., and Wong C. H., “On the study of elastic and plastic properties of multi-walled carbon nanotubes under axial tension using molecular dynamics simulation”, Acta Mater., vol. 52, pp. 2521(2004).

[48] Odegard G. M., Gates T. S., Nicholson L. M., and Wise K. E.,"Equivalent- continuum modeling with application to carbon nanotubes", NASA/TM-2002-211454,(2002).

[49] Li C. and Chou T. W., “A structural mechanics approach for the analysis of carbon nanotubes”, Int. J. Solids Struct., vol. 40, pp. 2487(2003).

[50] Chang T. and Gao, H., “Size-dependent elastic properties of a single-walled carbon nanotube via a molecular mechanics model”, J. Mech. Phys. Solids, vol. 51, pp. 1059(2003).

[51] Tserpes K. I., and Papanikos P., “Finite element modeling of single-walled carbon nanotubes”, Composites Part B, vol. 36,pp. 468(2005).

[52] K.I. Tserpes and P. Papanikos, “The effect of Stone–Wales defect on the tensile behavior and fracture of single-walled carbon nanotubes”, Comp. Struct., vol. 79, pp. 581–589 (2007)

[53] C.-W. Fan, J.-H. Huang, C. Hwu, Y.-Y. Liu, “Mechanial properties of single-walled carbon nanotubes- a finite element approach”Adv. Mater. Res., vol. 937, pp. 33–37,(2008).

[54]H. Wan, F. Delale, A structural.mechanics.approach.for.predicting.the.mechanical.properties of carbon.nanotubes”, Meccanica, vol. 45, pp. 43-51 (2009).

[55] Scarpa F., Adhikari S., and Wang C. Y., “Mechanical properties of non-reconstructed defective single-wall carbon nanotubes “, Journal of Physics D: Applied Physics, vol. 42, pp. 142002(2009)

[56] Xiaoa J. R., Staniszewskia J., Gillespie J. J. W.," Tensile behaviors of graphene sheets and carbon nanotubes with multiple Stone–Wales defects", Materials Science and Engineering A, vol. 527, pp. 715(2010)

[57] Allen M. P. and Tildesley D. J., Computer Simulation of Liquids, Oxford University Press, New York (1987).

[58] Rappe A. K., Casewit C. J., Colwell K. S., Goddard III W. A., and Skiff W. M., "UFF, a Full periodic table force field for molecular mechanics and molecular dynamics simulations" J. Am. Chem. Soc. 114, 10024(1992).

[59] Fan C. W., Liu Y. Y., and Hwu C., "Finite element simulation for estimating the mechanical properties of multi-walled carbon nanotubes", Appl Phys A, vol. 95, pp. 819(2009).

[60] Fung C. Y., Foundations of Solid Mechanics. Englewood Cliffs (NJ): Prentice-Hall (1965).

[61] Harik V. M., "Ranges of applicability for the continuum beam model in the mechanics of carbon nanotubes and nanorods", Solid State Commun., vol. 120,pp. 331(2001).

[62] Tsai S. W., Composites Design. Dayton OH: Think Composites Press (1988).

[63] Haile J. M., Molecular Dynamics Simulation: Elementary Methods, Wiley & Sons, New York (1992).

[64] Hoover W. G., Molecular Dynamics, Lecture Notes in Physics 258, Springer-Verlag, Berlin (1986).

[65] Rapaport D. C., The Art of Molecular Dynamics Simulation,1st Edition, Cambridge University Press, New York (1995).

[66] Rigby, D.; Sun, H.; Eichinger, B. E., "COMPASS: An Ab Initio Forcefield Optimized for Condensed-Phase Application-Overview with Details on Alkane and Benzene Compounds," Polym. Int., vol. 44, pp. 311(1997).

[67] Yakobson B. I., Brabec C. J., and Bernholc J., "Nanomechanics of Carbon Tubes: Instabilities beyond Linear Response", Phys. Rev. Lett., vol. 76, pp. 2511(1996).

[68] Zhou X., Zhou J., and Ou-Yang Z. C., "Strain energy and Young's modulus of single-wall carbon nanotubes calculated from electronic energy-band theory", Phys. Rev. B, vol. 62, pp. 13692(2000).

[69] Tu Z. C., and Ou-Yang Z. C., "Single-walled and multiwalled carbon nanotubes viewed as elastic tubes with the effective Young's moduli dependent on layer number", Phys. Rev. B, vol. 65, pp. 233407 (2002).

[70] Pantano A., Parks D. M., and Boyce M. C., "Mechanics of deformation of single- and multi-wall carbon nanotubes", J. Mech. Phys. Solids, vol. 52, pp. 789(2004).

[71] Hernández E., Goze C., Bernier P., and Rubio A., "Elastic Properties of C and BxCyNz Composite Nanotubes",Phys. Rev. Lett. 80, 4502–4505 (1998).

[72] Jin Y. and Yuan F. G., "Simulation of Elastic Properties of Single-Walled Carbon Nanotubes,"Compos.Sci. Technol., vol. 63, pp. 1507(2003).

[73] Lu J. P., "Elastic Properties of Carbon Nanotubes and Nanoropes", Phys. Rev. Lett., vol. 79, pp. 1297(1997).

[74] Gao X. L. and Li K.," Finite deformation continuum model for single-walled carbon nanotubes", Int. J. Solids Struct., vol. 40, pp. 7329(2003).

[75] Yao N. and Lordi V., “Young's modulus of single-walled carbon nanotubes”, J. Appl. Phys. vol. 84, pp. 1939(1998).

[76] Salvetat J. P., Briggs G. A. D., Bonard J. M., Bacsa R. R., Kulik A. J., Stöckli T. , Burnham N. A. , and Forró L., “Elastic and shear moduli of single-walled carbon nanotube ropes”,Phys. Rev.Lett. vol. 82, pp. 944(1999).

[77] Demczyk B. G., Wang Y. M., Cumings J., Hetman M., Han W., Zettl A., and Ritchie R. O., “Direct mechanical measurement of the tensile strength and elastic modulus of multiwalled carbon nanotubes”, Mater. Sci. Eng. A, vol. 334, pp. 173(2002).

[78] Yu M. F., Files B. S., Arepalli S., and Ruoff R. S., “Tensile loading of ropes of single wall carbon nanotubes and their mechanical properties”, Phys. Rev. Lett., vol. 84, pp. 5552(2000).

[79] Peacock A. J., Handbook of Polyethylene: Structures, Properties and Applications. New York (USA): Marcel Dekker Inc(2000).